Mechanisms facilitating uptake of carboxyl-polyethylene glycol-functionalised gold nanoparticles into multicellular spheroids

by

Seth-Frerich Fobian

Dissertation submitted in fulfilment of the requirements for the degree

Magister Scientiae

in

Pharmacology

Department of Pharmacology

School of Medicine

Faculty of Health Sciences

University of Pretoria

Supervisor

Prof. Werner Cordier

Co-supervisors

Prof. Vanessa Steenkamp

Prof. Mary Gulumian

February 2021

UNIVERSITEIT VAN PRETORIA
UNIVERSITY OF PRETORIA
YUNIBESITHI YA PRETORIA

Declaration

University of Pretoria

Faculty of Health Sciences

Department of Pharmacology

I, Seth-Frerich Fobian,

Student number: 15013252

Subject of work: Mechanisms facilitating uptake of carboxyl-polyethylene glycol-functionalised gold nanoparticles into multicellular spheroids

Declare that:

1. I understand what plagiarism is and am aware of the University's policy in this regard.
2. I declare that this project is my own original work. Where other people's work has been used (either from a printed source, internet, or any other source), this has been properly acknowledged and referenced in accordance with departmental requirements.
3. I have not used work previously produced by another student or any other person to hand in as my own.
4. I have not allowed and will not allow anyone to copy my work with the intention of passing it off as his or her own work.

Signature

.....

February 2021

Acknowledgements

The following are sincerely acknowledged for their support, be it scientific, technical, financial, or personal, throughout the duration of this study. Without you, none of this would have been possible.

Melissa Petzer – my lab partner and friend

Melissa Vetten – for technical (CytoViva) expertise and training

Margo Nell – for use of your laboratory space

Susra van Biljon – for use of the Cryostat in your laboratory

Andy Ellero – for endless advice, guidance, reagents, and equipment

Shirley and Ulrich Fobian – my parents, for giving me everything, and seeing me through my education

Ulrich and Hannah Fobian – my siblings, for paving the way for me to dream bigger

Savannah Fobian – my wife, for endless emotional support, friendship, and belief in me

Funding for experimentation is hereby acknowledged from Brazil, Russia, India, China, South Africa (BRICS) in conjunction with the National Research Foundation (NRF), as well as the University of Pretoria Postgraduate Master's Research Scholarship for a generous contribution to tuition fees.

"The fear of the Lord is the beginning of all wisdom; all who follow his precepts have good understanding. To Him belongs eternal praise." – Psalm 111:10

When I started this degree, I set out to write something, not that no one else *would* have written; rather, that no one else *could* have written, thereby bringing my uniqueness to my science. I hope that I have been successful in doing so. My admiration and reverence of the Lord Jesus has enabled me to produce this study.

"Sometimes, the best answer is a more interesting question"

-Terry Pratchett

Abstract

The drug discovery pipeline is hindered by confounding and non-representative *in vitro* cellular models. Traditionally, monolayer cell cultures have been used to evaluate drug toxicity and efficacy; however, are not sufficiently representative of the *in vivo* milieu. More advanced culture methods, including three-dimensional (3D) multicellular tumour spheroids, offer a solution by presenting a more appropriate physiological state for the cellular system. Equally damaging to the drug discovery pipeline, however, are candidate drug compounds with little potential. Nanomedicines have shown promise in drug delivery and various other theragnostic applications, and increasingly continue to do so. Generally, medicines are required to permeate structures, especially solid tumours, into the intracellular environment to exert activity. As such, there is a need for both uptake mechanisms and intracellular trafficking pathways to be well characterised. Further to the potential for cancer research, the National Institute for Occupational Health (South Africa) researches the Health, Safety, and Environment (HSE) of engineered nanomaterials. This study aimed to establish an A549 alveolar carcinoma spheroidal drug discovery and toxicity testing platform for the elucidation of uptake mechanisms employed for the pilot nanoparticles (NPs) in this study: 14 nm carboxyl-polyethylene glycol-functionalised gold nanoparticles (PCOOH-AuNPs).

The PCOOH-AuNPs were manufactured and characterised in terms of size, surface charge, spectral activity, and concentration by Mintek (South Africa). The A549 alveolar carcinoma cell line was used in conjunction with the liquid overlay technique, allowing for efficient and reproducible spheroid formation. Phase contrast microscopy was used alongside ImageJ analysis to monitor morphological aspects of spheroid growth, as well as cell lysis and lactate dehydrogenase (LDH) release for relative enumeration of cells. Live/dead staining was used to visualise areas of metabolic activity (viability) and compromised membranes (cell death) within a spheroid. Cytotoxicities of the PCOOH-AuNPs and pharmacological uptake inhibitors were assessed by monitoring LDH release from spheroids after exposure. Uptake mechanisms were assessed via CytoViva® hyperspectral imaging of 5 µm cryotomed spheroid sections after exposure to the pharmacological uptake inhibitors; sodium azide, dynasore, 5-(N-ethyl-N-isopropyl) amiloride (EIPA), genistein, and chlorpromazine.

Cells formed compact and reproducible spheroids within seven days after seeding, showing an average diameter and circularity index of 702.11 µm and 0.80, respectively. Zones of rapid metabolism and viability were evident from live/dead staining towards the superficial layers of a spheroid, as were zones of cell death towards the core of the spheroid. The Day 7 spheroids exhibited no greater LDH release than negative controls when exposed to either the AuNPs (2 and 24 h exposures) or pharmacological inhibitors (3 h exposures). Internalised AuNPs were counted in the presence or absence of uptake inhibitors to deduce employment of endocytic mechanisms. Counts were obtained and the following proportions of uptake mechanisms were calculated to have been employed for PCOOH-AuNP uptake: 9.2% passive diffusion, 6.6% macropinocytosis, 17.1% clathrin- and caveolae-independent pathways, 33.5% to 54.8% clathrin-mediated endocytosis, and 3.1% to 24.4% caveolae-mediated endocytosis. Penetration of AuNPs into spheroids was, on average, 4.5 µm, which is low, and indicates low levels of transcytosis, as well as intracellular retention of the PCOOH-AuNPs.

Uptake mechanisms employed by A549 spheroids for PCOOH-AuNPs were found to be diverse; however, primarily occurred via clathrin-mediated endocytosis. This means that PCOOH-AuNPs are likely to be trafficked towards a degradative fate in the lysosome. Such a destination largely invalidates their use for intracellular drug delivery, unless drugs or NPs are to induce lysosomal membrane permeabilization, exerting action in that way. Findings made in this study promise to inform intelligent design of future AuNP renditions having the goal of greater safety, efficacy, and achievement of desired theragnostic purpose. Further, the lack of cytotoxicity of both the PCOOH-AuNPs and all the uptake inhibitors, validates the methods in this study as reliable. A reproducible, representative 3D *in vitro* NP testing model has been established, using the A549 alveolar carcinoma cell line, which can be used to assess uptake strategies employed by NPs.

Table of Contents

List of abbreviations, units, and symbols

0-9	2D	Two-dimensional
	3D	Three-dimensional
A	APH	Acid phosphatase
	Arf1/6	Adenosine diphosphate-ribosylation factor 1/6
	ATP	Adenosine triphosphate
	ATPase	Adenosine triphosphatase
	ATCC	American Type Culture Collection
	Au	Gold
	AuNP	Gold nanoparticle
B	BEAS-2B	Human bronchial epithelial cell line
	BRICS	Brazil, Russia, India, China, South Africa
C	Cdc-42	Cell division control protein 42 homolog
	c-Myc	Myelocytomatosis
	CNT	Carbon nanotube
	CO_2	Carbon dioxide
	COOH	Carboxyl group
	CDK	Cyclin-dependent kinase
D	DCF	Dichlorofluorescein
	DCFH	Dichlorodihydrofluorescein
	dH_2O	Distilled water
	DMSO	Dimethyl sulfoxide
	DMEM	Dulbecco's Modified Eagle Medium
E	ECM	Extracellular matrix

	EDTA	Ethylenediaminetetraacetic acid
	EE	Early endosome
	EIPA	5-(N-ethyl-N-isopropyl) amiloride
F	FCS	Foetal calf serum
	FDA	Fluorescein diacetate
	FI	Fluorescence intensity
	Fig.	Figure
	FTA	Fluorescent treponemal antibody
G	*g*	Gravitational force
	g	Gram
	g/L	Gram per litre
	G1-phase	First mitotic growth phase
	GTP	Guanosine triphosphate
	GTPase	Guanosine triphosphatase
H	h	Hour
	HIF	Hypoxia-inducible factor
	HSI	Hyperspectral imaging
	hTF	Human transferrin
I	IC_{10}	Inhibitory concentration for 10% of a population
K	kV	Kilovolt
L	L	Litre
	LacCer	Lactosyl ceramide
	LDH	Lactate dehydrogenase
	LMP	Lysosomal membrane permeabilization

M	M	Molar
	MCTS	Multicellular tumour spheroids
	MDR	Multidrug resistance
	mg/mL	Milligrams per millilitre
	min	Minute
	mL	Millilitre
	mV	Millivolt
	MP	Macropinocytosis
	MTS	3-(4,5-dimethylthiazol-2-yl)-5-(3-carboxymethoxyphenyl)-2-(4-sulfophenyl)-2H-tetrazolium
	MTT	3-(4,5-dimethylthiazol-2-yl)-2,5-diphenyltetrazolium bromide
	MVB	Multivesicular bodies
N	NIOH	National Institute for Occupational Health
	nm	Nanometre
	nM	Nanomolar
	NP	Nanoparticle
O	O_2	Oxygen
	OD	Optical density
P	*p*	P-value for statistical significance
	PBS	Phosphate-buffered saline
	PCOOH	Carboxyl-polyethylene glycol
	PEG	Polyethylene glycol
	PEGylated	Polyethylene glycolated
	P-gp	P-glycoprotein

	pH	Power of hydrogen
	PI	Propidium iodide
R	®	Registered trademark
	R	South African Rand (ZAR)
	Rac1	Ras-related C3 botulinum toxin substrate 1
	RE	Recycling endosome
	RFU	Relative fluorescence units
	RhoA	Ras homolog gene family, member A
	rhTNF	Recombinant human tumour necrosis factor
	ROS	Reactive oxygen species
S	s	Second
	SAHPRA	South African Health Products Regulatory Authority
	SAM	Spectral angle mapping
	SDS	Sodium dodecyl sulphate
	S-phase	Mitotic synthesis phase
	SPION	Superparamagnetic iron oxide nanoparticles
	SV40	Simian virus 40
T	TEM	Transmission electron microscopy
	Tris-HCl	Trisaminomethane hydrochloride
	™	Trademark
U	UK	United Kingdom
	US$	American dollar
	USA	United States of America
W	WST-1	Water-soluble tetrazolium salts
	w/v	Weight per volume

X	XTT	2,3-bis-(2-methoxy-4-nitro-5-sulfophenyl)-2H-tetrazolium-5-carboxanilide

Symbols	α	Alpha
	β	Beta
	ζ	Zeta
	µg/mL	Microgram per millilitre
	µL	Microlitre
	µm	Micrometre
	µM	Micromolar
	π	Pi
	%	Percent
	°C	Degrees Celsius

List of Figures

List of Tables

Chapter 1: Literature Review

1.1 Introduction

The drug discovery pipeline, in accordance with both the South African Health Products Regulatory Authority (SAHPRA) and global regulatory authorities,[1,2] begins with the identification of novel compounds with possible therapeutic potential.[3] Compounds are screened using *in vitro* assays evaluating their efficacy, safety, and proposed target(s).[4,5] The results generated from such *in vitro* assessments are leveraged in the motivation for or against a compound's progression to the subsequent phases of the pipeline, namely, *in vivo* testing, followed by clinical trials in humans.[5] *In vivo* methods are conducted in physiologically, anatomically, or metabolically similar animals such as mice, rats, and pigs,[6] after which a potential drug would enter phases I to IV of clinical trials.[1] Should a favourable efficacy and safety profile be observed, the drug is placed on the pharmaceutical market. On average, US$ 1-2.5 billion and approximately 10 years are spent on the development of a single new chemical entity, regardless of market entry.[7,8]

Although it is clear that more efficient and accurate inaugural modalities for this pipeline are necessary, many such models have yet to be developed or adopted.[9] *In vitro* methods frequently produce findings that are inconclusive, irrelevant, or even contrary to those observed subsequently.[9] The earlier on in the pipeline a researcher can halt a potential drug's development, the less costly and more robust the process becomes. This could be achieved through improvements to the initial *in vitro* screening and mechanistic evaluations of a new compound, such as the use of more reliable *in vivo*-representative *in vitro* platforms.[4,10] Models with greater representation of the physiological system hold promise for more successful efficacy and safety testing, reduction in spending of both time and money, and generation of more reliable results.[3]

The current global climate of cancer drug research exemplifies the above. High attrition rates plague cancer research, which remain a hurdle in the pharmaceutical industry, with market authorisation being granted to as low as 5% of potential anticancer drugs enrolled in phase I clinical trials.[10,11] Attrition refers to the removal of a candidate drug from pre-clinical and/or

clinical steps of the pipeline due to i) severe toxicity, most commonly (in descending order) hepatic, cardiovascular, and haematological,[12] and/or ii) a lack of efficacy.[3,10]

1.2 Spheroids as a solution to failing *in vitro* techniques

1.2.1 *In vivo* representation

Multicellular tumour spheroids (MCTS) may bridge the gap between *in vitro* and *in vivo* systems.[13] Spheroids offer a simple, reproducible and more representative model,[7] as they more appropriately simulate the tumour microenvironment's cellular complexity,[14] and enhance the predictive capability of *in vitro* systems.[15] The superiority of three-dimensional (3D) cell culture models over two-dimensional (2D) culture models is well-documented.[15-18] Functional and morphological mimicry by spheroids of living tissues increases the relevance of cytotoxicity and mechanistic data generated *in vitro*.[15,16,19] The aforementioned characteristics include cell-cell and cell-matrix interactions, metabolic gradients, viability, differentiation, gene regulation, and cell cycle control.[16] Applications of 3D culture models include differentiation and expression studies, drug discovery, pharmacological mechanistic evaluation and cancer research, all of which would benefit greatly from a more representative model of the *in vivo* environment than the 2D counterpart.[20]

1.2.2 Spheroid formation

Spheroid formation, unlike traditional 2D monolayer cultures, depends on the adhesion of cultured cells to each other rather than to the culture vessel.[21] When adherent cells aggregate with one another,[22] the adhesion protein cadherin accumulates extracellularly on the membrane surface, followed by homophilic cadherin-cadherin binding, allowing for the formation of compacted spheroids.[21] Cadherin-cadherin interactions lead to the deposition of extracellular matrix (ECM),[21] marked by a smooth surface on the spheroid with no distinguishable single cells (Fig. 1.1).[23] Additionally, E-cadherin has been shown to initiate transcription of the proteins cyclin D1 and the proto-oncogene and regulator of cell cycle entry, c-Myc, which together, promote the transition of cells from the G1 to S-phase of mitosis, enhancing proliferation to an extent.[21,24] Cell-cell interactions are more prominent in spheroids than cell-substrate interactions.[7]

Spheroids deposit ECM, which, in conjunction with functional and morphological characteristics, opposes the unrestrained proliferation observed in 2D monolayer cultures.[4] The presence of ECM is necessary for *in vitro* emulation of characteristic *in vivo* cell-cell and cell-matrix interactions.[21,22] The dynamic, non-cellular network known as ECM (Fig. 1.1) comprises collagen, proteoglycans, glycosaminoglycans, enzymes, elastin, fibronectin, laminin, and other glycoproteins secreted by cells.[25] It provides mechanical structure to tissues; facilitates adhesion and homeostasis, and regulates cellular migration, proliferation and differentiation.[25-27]

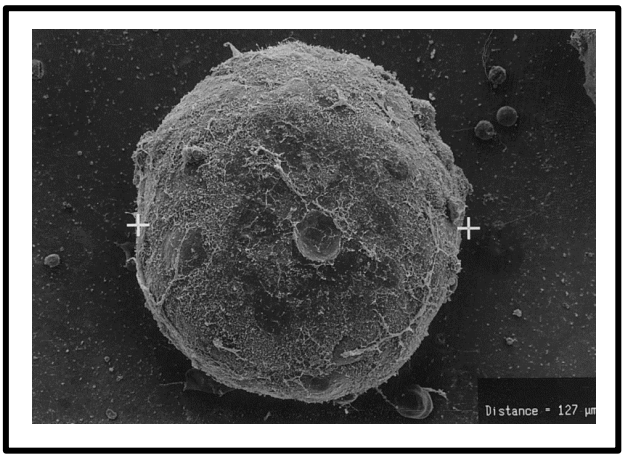

Fig. 1.1: Scanning electron micrograph demonstrating deposition of extracellular matrix in a fully-formed, compacted A431 squamous carcinoma spheroid.[23] Reprinted from Critical Reviews in Oncology/Hematology, Vol 36, Maria Teresa Santini, Gabriella Rainaldi, Pietro Luigi Indovina, Apoptosis, cell adhesion and the extracellular matrix in the three-dimensional growth of multicellular tumor spheroids, Pages No. 75-87, Copyright (2000), with permission from Elsevier.

1.2.3 Spheroid morphology

Spheroids display many morphological similarities to *in vivo* tumours, such as differential zonation, leading to a characteristic external proliferative zone, an internal quiescent zone, and a necrotic core.[4] Such zones develop due to poor perfusion of oxygen, nutrients and metabolites from the environment through these cellular and ECM layers, as well as accumulation of metabolic waste products within.[4,13] As such, hypoxia, pH levels, cellular debris, and nutrient availability all occur according to gradients (Fig. 1.2).[4,28] The extent of perfusion may be affected by the density of the cell packing within the spheroid, highlighting the importance of reproducibility in cell culture methods.[4]

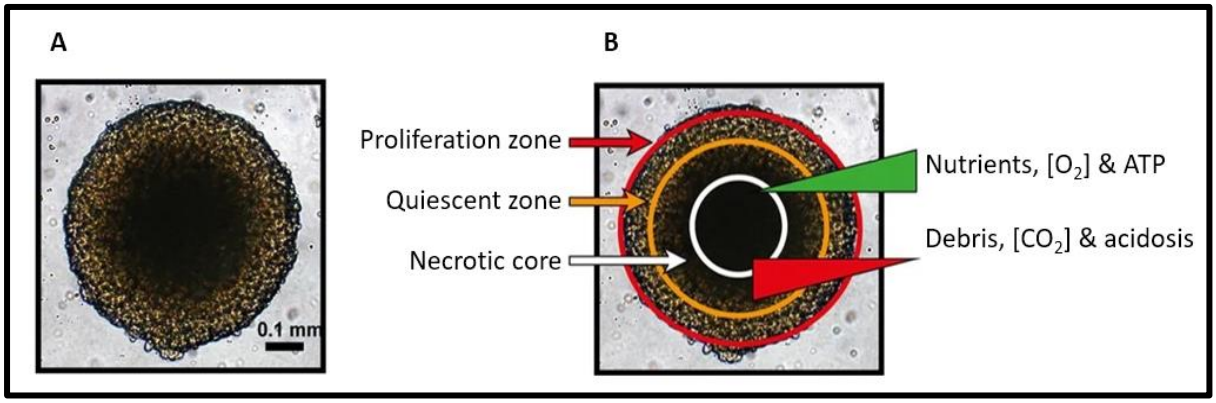

Fig. 1.2: Brightfield image of A549 spheroid (A) with a schematic representation of nutrient gradients (B). Gradients exist due to poor perfusion of nutrient through the densely packed cellular layers of a spheroid. Scale bar defined as 0.1 mm.[4] Abbreviations: [O_2]; oxygen concentration, [CO_2]; carbon dioxide concentration, ATP; adenosine triphosphate. Use of this figure is authorised under terms of the Creative Commons CC BY licence.

Expression of certain membrane transporters, such as the P-glycoprotein (P-gp) multidrug resistance (MDR) efflux pump, is proportionally linked to the presence and extent of the quiescent and hypoxic zones.[29] Hypoxia in the spheroid's core correlates to increased expression of hypoxia-inducible factor (HIF)-1α,[30] which up-regulates P-gp expression and increases the likelihood of endocytosed drugs or molecules to be removed from the intracellular compartment before exerting biological activity.[30] Additionally, as observed *in vivo*, drug penetration is poorer in spheroids.[4] These factors contribute to spheroids' higher resistance to cytotoxic drugs (including chemotherapeutic, immunotherapeutic, radiation, and antibody treatments) than monolayer cultures of the same cell line.[29,31]

1.2.4 Three-dimensional cell culture methods

Separate testing and optimisation are recommended for different cell types and experiments, because each method presents unique capabilities and limitations.[32] Specific assay and/or cell line selections motivate for the selection of certain culture methods.[22,33] There are several methods available for 3D cell culturing, generally divided by the use of liquid- or scaffold-based models.[22]

Liquid-based models, also known as scaffold-free models, either allow for cells to self-assemble or force them to cluster together.[4] These include the hanging drop and liquid overlay techniques.[22] The hanging drop technique relies on specialised plates which suspend a drop of liquid medium and cell suspension from a surface, preventing attachment of cells to any substrate, thus encouraging cell aggregation and spheroid formation.[22] The A549 cell

line (used in this study) has successfully been grown as spheroids within 72 h, using the liquid overlay method,[32] and Corning® Ultra-Low Attachment (ULA) plates (possessing a covalently-bound hydrogel layer to inhibit attachment to the plates).[22,33] These methods cause spheroids to form reproducibly when cells are seeded into concave wells coated with anti-adhesive polymers like agarose, which can also be blended with growth media elements.[33]

Scaffold-based 3D models use natural or synthetic physical or chemical support systems that reproduce *in vivo* conditions[4] with a supportive extracellular environment.[22] Scaffold design must closely replicate tissue type of interest, and includes porous materials of specific size and shape, allowing representative growth and distribution of gases, metabolites, and nutrients.[22] This can be achieved using metal, glass, polymers (plastic-like materials), or ceramics.[34] Biocompatible polymers such as poly-glycolic acid, poly-lactic acid, chitosan and collagen can also be added to alter chemical environment in favour of aggregation, attachment, and/or growth.[22,34] While scaffolds offer the possibility for increasing throughput, reproducibility, and allowing tighter chemical control of a cell culture system,[22] they were not suitable to this study for two reasons. Firstly, scaffolds become necessary for growing larger, complex cultures of 1-2 mm in size.[22] Secondly, scaffold-based techniques introduce diversity and variation in experimental techniques.[34] For the purposes of this study, scaffold-free generation methods were more appropriate to answer the research question, and permitted better reproducibility and comparability.

1.3 Nanoparticles and nanomedicine

1.3.1 Nanoparticles

The second point of departure in the improvement of the drug discovery pipeline lies with improving the chemical compounds being assessed. The primary shortfall of many allopathic drugs is that they exhibit action while circulating in the bloodstream.[35] Thus, it becomes necessary for a higher overall concentration of the drug to be administered in an attempt to increase the concentration of the drug at the site of disease, injury, or infection.[35] Chemotherapeutic drugs, in particular, are also typically non-specific, rapidly metabolised and/or excreted, and do not accumulate at tumour sites.[28,36] The lack of specificity leads to cytotoxicity towards various types of rapidly dividing cells, including macrophages, hair

follicles, and those of the bone marrow and alimentary canal,[37] increasing the incidence of systemic adverse effects.[35] The latter is of concern, particularly in cancer chemotherapy, with adverse effects including fatigue, increased susceptibility to infections, nausea, vomiting, alopecia, and others, ranging in severity.[38]

Nanomedicine, the field involving the use of nanomaterials in medical applications, has seen immense growth in recent years.[36] This is partially due to nanomaterials' potential as agents capable of targeted therapy via conjugation of tumour-specific biomarker ligands to nanoparticle (NP) surfaces, as well as alterations to NP surface chemistry.[35] Such modifications enable drug-conjugated NPs to concentrate at certain tissues or cells and allow a reduced systemic drug concentration to achieve similar efficacy.[35,39] Nanoparticles can also prevent premature degradation of drugs.[36] These factors collectively improve the therapeutic index and increase the bioavailability of drugs, improving the safety and efficacy profiles of conventional therapies.[36] If these principles are applied in nanomedicine, patients can benefit from the same therapeutic efficacy with administration of lower drug doses, significantly increasing quality of life by way of lessening the incidence of adverse effects.[35,40]

Engineered nanoparticles are synthetic materials of between 1 and 100 nm in size,[41] that can be synthesised through processes allowing fundamental control over chemical and physical properties.[42] Therefore, by design, aspects including chemical composition (type), size, shape, surface chemistry, charge, and conjugates can be controlled to produce NPs to exact specification for intended use.[41,43] Nanomedicines typically exhibit low toxicity and high biocompatibility relative to conventional therapies.[44] Nanoparticles and nanomedicines are currently being studied for application in diagnostics (visualisation and bioimaging), immunology (vaccines, biodistribution, and cytotoxicity), and therapeutics (drug/gene delivery, anti-angiogenesis, as well as radiofrequency and photothermal therapy).[45-48] Types of NPs that are of interest in nanomedicine[49] include: for imaging, quantum dots and superparamagnetic iron oxide NPs (SPIONs); for theranostics, carbon nanotubes (CNTs) and silica NPs, and for drug delivery, liposomes, dendrimers, and nanogels, among others.[49]

Gold nanoparticles have shown applicability in all of the aforementioned areas,[40,45,48,50] making them very appealing candidates for nanomedical research, especially those between

10 and 100 nm.[51] At the nanoscale level, the particles' surface area-to-volume ratio is much greater compared to larger-scale counterparts, which alters their chemical and physical properties.[52] For example, bulk gold is considered an inert metal, but in the form of NPs, catalytic activity is exhibited which is utilised in nanomedicine.[52]

1.3.2 Nanoparticles in this study

Recently, 14 nm polyethylene glycol (PEG)-coated (PEGylated) gold nanoparticles (AuNPs) with carboxyl (COOH) functionalisation (Mintek, Randburg, South Africa) were studied at the National Institute for Occupational Health (NIOH, Johannesburg) by Gulumian and colleagues (University of the Witwatersrand, Johannesburg). These PCOOH-AuNPs have a molecular weight of 526.73 g/mol and possess a carboxyl group conjugated to a PEG chain (Fig. 1.3).[50] These specific PCOOH-AuNPs exhibited low cytotoxicity and were taken up by the bronchial epithelial cell line BEAS-2B contrary to non-carboxylated PEGylated AuNPs, where no uptake occurred.[50] Thus, functionalisation improved the uptake properties of the AuNPs.

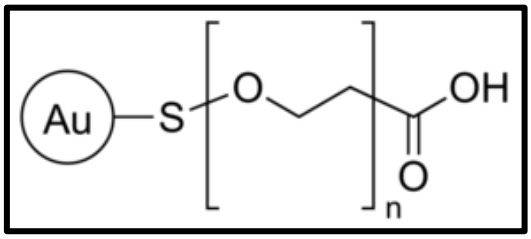

Fig. 1.3: Chemical structure of carboxyl-PEG-functionalised AuNPs. Where "n" denotes repeating ethylene glycol groups and "(Au)" denotes the gold nanoparticle. Image courtesy of Merck (Darmstadt, Germany).

A recent example of AuNPs being studied for therapeutic use, as discussed in Section 1.3.1, is documented in a clinical trial by Libutti *et al.*[53,54] Solid tumours were treated with recombinant human tumour necrosis factor (rhTNF) bound by a PEG-linker to AuNPs.[54] The AuNPs served secondarily as an antifouling agent, but primarily as a targeting agent. The rhTNF-AuNP conjugate could be administered at triple the dose of free rhTNF without causing toxicity.[53,54] Apart from drug delivery, inherent anticancer activity (reactive oxygen species [ROS]-induction and anti-angiogenesis) of AuNPs has also been noted.[40,48,55] There are many other AuNP-based nanomedicines which may have worthwhile therapeutic potential, particularly in cancer treatment.[40,48,56-58] Sztandera *et al.* noted the therapeutic superiority and heightened potential of AuNPs when compared to other nanomatierials.[40] For example, lysosomal membrane permeabilization (LMP) has been induced by AuNPs.[59] As a mechanism

of cytotoxicity for cancer cells, LMP can be considered, causing leakage of degradative lysosomal enzymes into the cytoplasm and subsequent autophagy.[55]

1.4 Cellular uptake

Spheroids' more accurate *in vivo* representation increases their feasibility for the study of uptake mechanisms and both inter- and intracellular trafficking.[35] This is especially true when considering NPs for drug delivery and targeting – the way in which the drug enters the cell must be well characterised.[60] Cellular uptake is necessary for many cellular functions, including hormone-mediated signal transduction, immune surveillance, antigen-presentation, and homeostasis; thus, mediating most of the cells' responses to environmental stimuli.[61] This includes responses to pharmacological agents and potential drugs: greatly hindered biological activity ensues from a lack of access to the intracellular environment, depending on the mechanism of action of the agent.[37] Various uptake mechanisms have been observed; however, it is known that most macromolecules and external particles gain entry to the intracellular environment by endocytosis.[62] During endocytosis, external molecules are surrounded by membrane-bound vesicles originating from invagination and clamping-off of the plasma membrane.[62] That being said, many mechanisms are still not clearly elucidated, such as the uptake of the NPs, and the intracellular destination of particles taken up.[62] An understanding of uptake pathways and the way they interact is crucial in understanding the intracellular targeting and therapeutic potential of any candidate drug or drug-delivery agent.[55,63]

1.4.1 Uptake mechanisms employed for NPs

Nanoparticle uptake is primarily via active endocytic pathways (most prominently, clathrin-mediated); however, some other pathways, including passive diffusion, may contribute.[50,61,64-66] Passive processes have been shown to occur in NPs of <200 nm in size.[67] These observations are widely regarded to have been made without comprehensive understandings of either uptake mechanisms or NPs, necessitating further research.[35,62,68] Certain endocytic pathways' effector proteins and control factors are also poorly understood, hindering *in vitro* experimentation.[35] Further problems arise such as a lack of standardisation or normalisation across studies concerning spheroid generation techniques, NP solubility in

different media, non-specific serum protein adsorption, varying responses from different cell types, non-reproducible NP-surface properties and varying experimental conditions.[68] Two major divisions of the endocytic pathways exist in mammalian cells to take up particles and macromolecules from the extracellular environment: phagocytosis and pinocytosis (Fig. 1.4).[61,68]

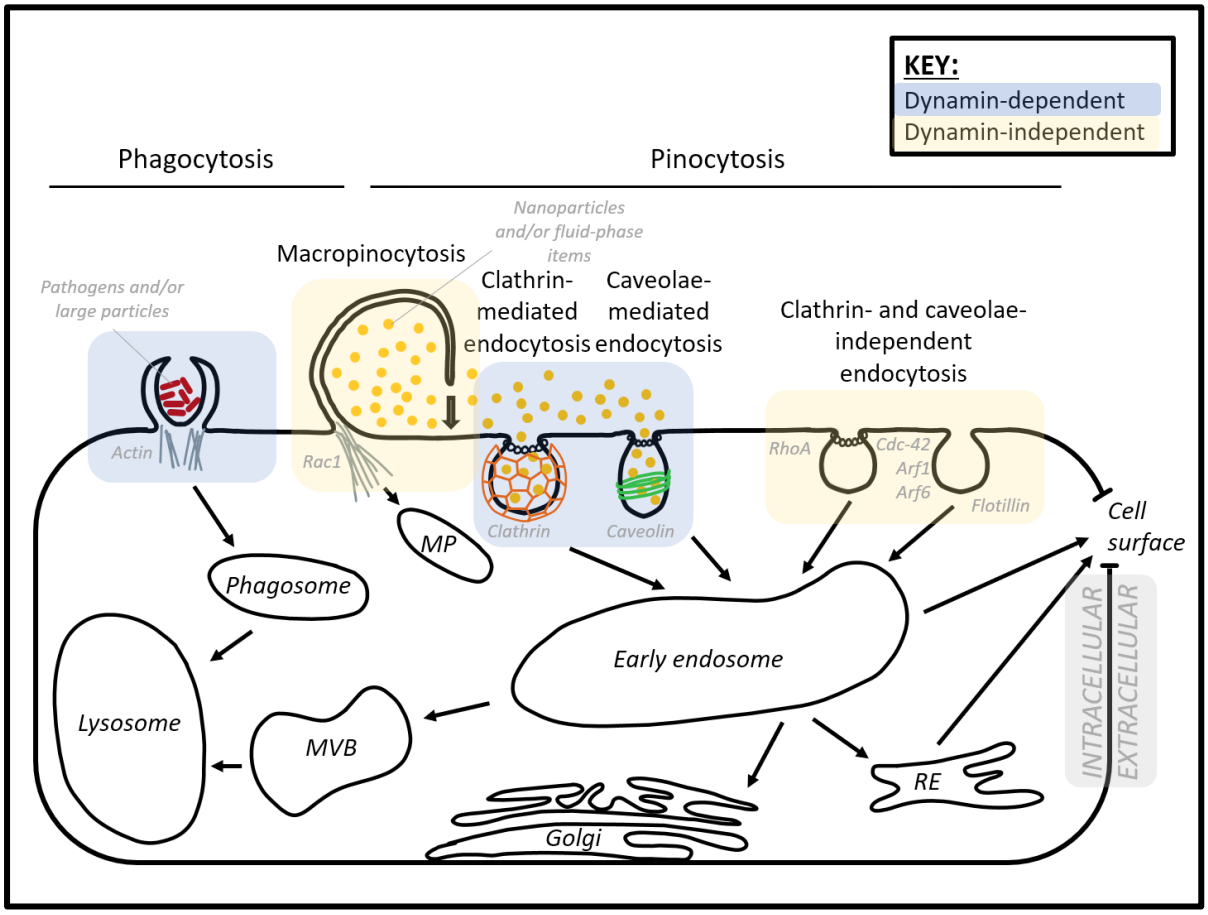

Fig. 1.4: The major endocytic pathways of a hypothetical cell and intracellular trafficking mechanisms, differing based on size, shape, charge, and phase of the external particles, as well as proteins involved.[61,62,69] Abbreviations: RE; recycling endosome, MVB; multivesicular body, MP; macropinosome, Rac1; ras-related C3 botulinum toxin substrate 1, RhoA; ras homolog gene family member A, Cdc-42; cell division control protein 42 homolog, Arf1/6; ADP-ribosylation factor 1/6. Original graphic.[61,62]

1.4.1.1 Phagocytosis

Phagocytosis occurs predominantly in specialised cells such as macrophages, monocytes, and neutrophils.[61] The primary function thereof is clearance of large particles (such as cellular debris) and pathogens, including bacteria and yeast.[61] These particles are trafficked intracellularly to phagosomes and lysosomes where inflammatory processes are initiated.[35] Thus, phagocytosis is crucial to the immune response.[35] Once within lysosomes, particles are enzymatically broken down in the presence of high concentrations of ROS and low pH (4.5-

5.0).[35,61,70] For phagocytosed NPs to exhibit activity, opsonins such as immunoglobulins or complement proteins must be conjugated externally for lysosomal degradation.[35] This process can be utilised in the case of proteinaceous NP drug-delivery systems, where proteolytic degradation would be required for activity,[62] or release could be triggered by low pH in the lysosome.[71]

1.4.1.2 Pinocytosis

Pinocytosis is the fluid-phase uptake of solutions and suspensions containing small particles. It is executed by four main divisions of pathways,[35] namely i) macropinocytosis, ii) clathrin-mediated endocytosis, iii) caveolae-mediated endocytosis, and iv) clathrin- and caveolin-independent pathways.[35,68]

i) Macropinocytosis

Macropinocytosis is non-specific enclosure of fluid pockets near the cell surface by membrane protrusions.[35,68] These actin-driven protrusions begin as membrane ruffles initiated by environmental stimuli.[35] Fully formed circular ruffles, known as lamellipodia, retract back onto the cell and fuse with the membrane,[72] resulting in packaging of engulfed particles into large vacuoles, then macropinosomes, endosomes, and lysosomes (for degradation).[73] As mentioned, other clathrin- and caveolae-independent endocytic pathways exist, which function in neuronal and neuroendocrine cells.[61,68] While poorly understood mechanistically, it has been shown that these pathways rely on cholesterol and other specific lipid compositions, as well as dynamin for control.[35]

ii) Caveolae-mediated endocytosis

Caveolae- and especially clathrin-mediated endocytosis (as well as phagocytosis and macropinocytosis) are of greatest relevance to NP uptake in spheroids.[62,74] In culture media, serum proteins are adsorbed to the NP surface, leading to receptor-mediated endocytosis.[68] Caveolae demarcate cholesterol- and sphingolipid-rich microdomains of the plasma membrane and function primarily in signal transduction.[61] As a scaffold, they possess caveolin; a transmembrane protein able to induce invaginations through oligomerisation.[75] Pathogens, toxins, and various other particles (including nanomaterials) interact with surface receptors to induce flask-shaped vesicles which are separated from the membrane by

dynamin.[35] Intracellularly, the caveolae fuse with caveosomes or multivesicular bodies (at non-degradative neutral pH) and thereafter, with early endosomes (EE).[35] From the EE, endocytosed particles are believed to penetrate into the cytosol, then to the nucleus through the nuclear pore complex.[76] Particles delivered this way avoid a degradative fate, enhancing potential for organelle-targeted delivery.[35] For this reason, nanomedicines, when used as nanocarriers, are being designed to target non-degradative caveolae-mediated endocytosis.[55] In these cases, enzyme-sensitive drugs can be shielded from the degradative environment of the lysosome.[77]

iii) Clathrin-mediated endocytosis

Clathrin-mediated endocytosis occurs slightly faster and makes use of smaller vesicles than its caveolae-mediated counterpart described above.[35] Clathrin is involved in the formation of coated pits, or cages (due to its triskelion structure) around invaginations.[61] These invaginations are brought about by cytosolic coat proteins following clathrin polymerisation in response to receptor interaction.[35,61] Clathrin-mediated endocytosis, among other processes, is responsible for internalisation of receptor-ligand complexes into the cell.[61] Dynamin pinches off invaginations to form clathrin-coated vesicles, which may fuse with lysosomes for degradation,[55] or be cycled back to the cell surface, depending on the receptor that was initially activated.[78] Vesicles formed as a result of clathrin- and caveolae-mediated endocytosis require actin and intact microtubules for intracellular movement and trafficking along the cytoskeleton.[35]

iv) Clathrin- and caveolae-independent endocytosis

Pathways not functionally dependent on clathrin, caveolae or even dynamin show involvement in some immunological functions (interleukin-2 receptors on lymphocytes), neurons, and neuroendocrine cells (membrane protein recovery after stimulated secretion).[61,79] This is proven by the fact that dynamin-mutant-mediated dynamin inhibition continues to allow fluid-phase uptake to take place.[61] Clathrin- and caveolae-independent pathways could play a supportive or ancillary role.[80] Fluid-phase endocytosis was observed 30-60 min after temperature-sensitive dynamin inhibition, and not before.[80] Upregulation

signals as well as governing mechanisms are still rudimentarily understood, but these pathways are thought to have evolved for the purpose of precise physiological coordination.[61]

1.4.2 Physicochemical properties of nanoparticles which affect uptake

A tiered approach in NP research has been proposed and widely adopted,[81] whereby physicochemical properties of the relevant NPs are characterised before commencing with *in vitro* and *in vivo* testing.[82] This is necessary following the discovery that the type and physicochemical properties of NPs can greatly impact cellular uptake and membrane interactions,[41,62,68,83] which affect downstream toxicity and/or therapeutic efficacy.[82] Nanoparticle size, shape, charge, and surface chemistry (also known as functionalisation) are of relevance here.[68]

1.4.2.1 Size

Chitrani *et al.*[43] and Malugin *et al.*,[84] in agreement with other authors,[62,85] have determined that the cellular uptake of AuNPs is optimal at a diameter of between 40 and 50 nm. Accordingly, Wang *et al*.[86] found that in comparison to larger NPs (75 nm), 45 nm AuNPs are endocytosed and trafficked to endosomes at a higher rate, making them ideal for drug delivery and internalisation. This was confirmed by Huo *et al.*[87] who found that 50 nm AuNPs were able to penetrate deeply into spheroids, while 100 nm AuNPs localised in the spheroid periphery. The size of NPs can affect the cellular uptake mechanism employed by the cell.[35,86] For example, clathrin-coated pits tend to measure around 100 nm and caveolae between 60-80 nm.[78] These structures respectively engulf NPs of appropriate sizes after taking into account the hydrodynamic diameter in culture media.[78] Hydrodynamic diameter accounts for the NP core, shell, and adsorbed culture media/serum proteins (forming a protein corona around the NP), enlarging them by approximately 25 nm.[74,87] Larger NPs are engulfed by phagocytosis or macropinocytosis.[35]

1.4.2.2 Shape

Nanoparticle shape also plays a role in extent and rate of uptake into cells.[35] Malugin *et al.*[84] noted that spherical NPs are taken up at a higher rate than rod-shaped NPs by human lung epithelial cells, which was corroborated by Chithrani *et al*.[43] However, rod-shaped NPs were able to enter macrophages more efficiently than non-immunogenic cells.[60] Rounder NPs tend

to face less resistance when considering entry into the cell, as aspect ratio and orientation (in relation to the cell membrane) have no effect.[60,66] Sharper edges result in suppressed endocytosis.[66]

1.4.2.3 Surface chemistry and functionalisation

Surface chemistry and functionalisation (and by extension, charge) of a NP also impact the rate and extent of endocytosis.[84] In 3D culture models, positively charged NPs are only taken up by viable cells, requiring active processes, while negatively charged NPs can diffuse more easily into deeper tissues.[88] It has been shown that functionalisation influences environmental interactions and stability of NPs.[89] Polyethylene glycol (PEG), for example, is a ligand which increases biocompatibility, enabling NPs to show low toxicity and function within appropriate biological requirements.[89] Its amphiphilicity increases NP solubility in a wider range of solvents.[41] However, in many cases, PEGylated NPs have exhibited significantly lower or no uptake when compared to their otherwise-functionalised or uncoated counterparts.[50,84] In some cases, adjustments to ligands in addition to PEG have resulted in increased uptake.[50] Thus, per findings by Vetten *et al.*,[50] carboxy-PEG (PCOOH)-functionalised NPs were the subject of this study.

1.4.3 Methods for studying uptake pathways

Given the diversity of uptake mechanisms, several modalities have been described for the study of these processes.[35] In conjunction with microscopy, the two broad ways to study uptake are using either fluorescent markers or inhibitors.[35] For more compelling and thorough results, these methods can be used in conjunction with one another, as discussed below.[35]

1.4.3.1 Molecular markers

Fluorescent markers or tags can be conjugated to NPs, allowing detection of endocytosed NPs by 2D or 3D confocal microscopy.[35] Commonly used markers include fluorescently-tagged low-density lipoprotein and transferrin, cholera toxin beta subunit, Shiga toxin, and dextran for clathrin-mediated endocytosis, caveolae-dependent endocytosis, and macropinocytosis, respectively.[35,90] Furthermore, fluorescently-tagged human transferrin (hTF) and lactosylceramide (LacCer) are taken up by clathrin-dependent and clathrin-independent

mechanisms, respectively.[90] Given the autofluorescent nature of NPs, marker-free approaches are also used.[91]

1.4.3.2 Inhibition of uptake

Uptake inhibition assays are powerful tools for elucidating mechanisms by which molecules of interest enter the intracellular environment.[62] Distinctions can be made between active, ATP-dependent endocytic mechanisms and other methods like passive diffusion by using ATPase inhibitors or by lowering incubation temperature.[35] Alternatively, based on the inhibition of a particular gamut of proteins involved in a certain uptake pathway (Fig. 1.4), specific mechanisms of cellular uptake can be studied.[62]

Certain NPs' autofluorescence and/or optical activity can cause interference with assays in various ways; however, these characteristics can be leveraged in certain methods such as fluorescence microscopy and flow cytometry, where, following optimisation, wavelengths at which the NPs are detectable can be used to assess cellular uptake and intracellular localisation without using dyes.[82] Commonly used pharmacological inhibitors are summarised in Table 1.1.

Table 1.1: Pharmacological inhibitors utilised in the study of endocytosis (adapted from Iversen et al.).[35,62,90,92]

Inhibitor	Mechanism of action	Uptake mechanism inhibited
Amiloride[62]	Lowers pH proximal to the inside of the membrane and inhibits Rac1 and Cdc-42	Macropinocytosis
Chlorpromazine[62,90]	Inhibits Rho GTPase	Clathrin-mediated endocytosis
Cytochalasin D[62]	Inhibits actin polymerisation and disrupts actin filaments	Macropinocytosis and possible others
Dynasore[62]	Dynamin inhibitor	Dynamin-dependent processes
EIPA[92,93]	F-actin reorganisation and pseudopodia retraction	Macropinocytosis and phagocytosis
Genistein[62,90]	Tyrosine kinase inhibitor with local disruption of actin network and inhibition of dynamin recruitment	Caveolae-mediated endocytosis (somewhat non-specific)
Jasplakinolide[62]	Stabilises actin and prevents its assembly.	Macropinocytosis
Latrunculin A[62]	Inhibits actin polymerisation and disrupts actin filaments	Macropinocytosis and other possible mechanisms
Lovostatin/Nystatin[62]	Down-regulating cholesterol synthesis	Possibly cholesterol-dependent processes
Methyl-β-cyclodextrin[62,90]	Cholesterol extraction from membrane	Macropinocytosis, clathrin-dependent, and clathrin-independent endocytosis
Phosphoinositide 3-kinase inhibitors[62]	Inhibits phosphatidylinositol 3-kinase	Macropinocytosis and RhoA-mediated endocytic mechanisms
Potassium depletion buffers[35]	Dissociates clathrin lattices beneath plasma membrane	Clathrin-mediated endocytosis
Sodium azide[35]	ATPase inhibitor	All endocytic pathways

Abbreviations: EIPA; 5-(N-ethyl-N-isopropyl) amiloride, Rac1; Ras-related C3 botulinum toxin substrate 1, Cdc-42: Cell division control protein 42 homolog, Rho GTPase; Ras homologous guanosine triphosphatase.

1.4.3.3 CytoViva® hyperspectral imaging

It is unfavourable to use dyes and pharmacological inhibitors simultaneously, as inhibitors may act on mechanisms by which dyes need to gain entry to the cells, skewing results. Thus, hyperspectral microscopy was used in conjunction with pharmacological inhibitors for determination of the uptake mechanism used by cells for PCOOH-AuNPs.[50] The CytoViva® system combines optical microscopy and spectrophotometry to enable spectral mapping of up to nanoscale images.[94] Spectral information is then integrated onto the image to be viewed directly in the spatial context of the optical image, enabling imaging of unprecedented contrast and resolution (Fig. 1.5).[94] Percentage uptake of PCOOH-AuNPs as per surface area of a micrograph can be determined, yielding semi-quantitative uptake results relative to initial NP dose. This has been used as an indirect method for determination of the extents of NP uptake.[82] Transmission electron microscopy (TEM) may serve as an alternative to hyperspectral imaging to study NP uptake and intracellular localisation should further information be desired.[95]

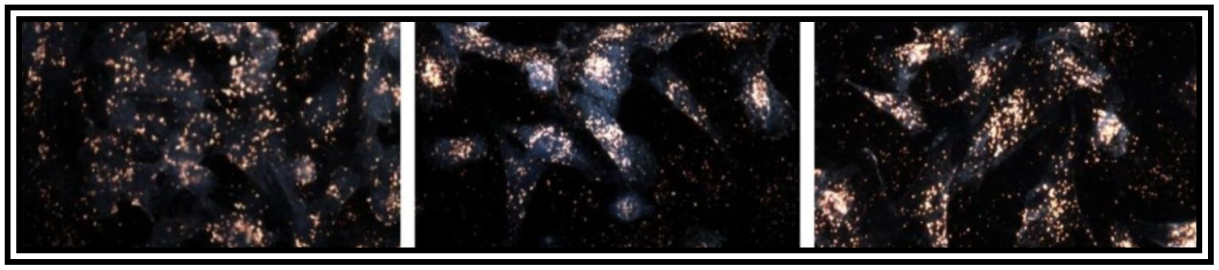

Fig. 1.5: An example of the images obtained using the CytoViva® system in BEAS-2B monolayer cultures after exposure to gold nanoparticles.[82] Reprinted with permission from Springer Nature: Springer, Particle and Fibre Toxicology, Label-free in vitro toxicity and uptake assessment of citrate stabilised gold nanoparticles in three cell lines, Vetten et al., copyright (2013).

1.5 Nanoparticle cytotoxicity

Gold nanoparticles possess inherent cytotoxicity,[82] often altered or modulated by characteristics such as size and surface functionalisation, and primarily exerted by intracellular induction of reactive oxygen species (ROS)[44] and ion release.[96] Uboldi *et al*. reported dose- and time-dependent cytotoxicity in the A549 cell line after exposure to AuNPs of sizes 9.5 to 25 nm, showing viability of cells to be 50% less after 72 h exposure when compared to 24 h exposure periods.[97] Alkilany *et al.*[98] and Pan *et al.*[99] both reported relatively low cytotoxicity from AuNPs between 5 and 15 nm in size. In other investigations, PEG-functionalised AuNPs have been found to show lower cytotoxicity than otherwise-

functionalised or bare AuNPs.[100,101] However, findings tend to be inconsistent, given the wide range of designer NPs being tested, as well as unstandardised or non-uniform experimental conditions.[102] This is the case with the above-mentioned studies: cytotoxicity testing methods included 3-(4,5-dimethylthiazol-2-yl)-2,5-diphenyltetrazolium bromide (MTT) and xCELLigence™ real-time cell analyser (Santa Clara, CA, USA), which could have influenced the results obtained. Thus, potential interferences are addressed in Section 1.5.2.

1.5.1 Methods for cytotoxicity assessment

Optimal methods need to be selected for applicability to both spheroid cell culture and NPs. Nath *et al.* noted that if spheroids are detached or disrupted into single-cell suspension, then cell viability could be affected.[103] This necessitates the use of methods applicable to intact spheroids for measurement of cell viability.[103]

Multiple research teams have successfully investigated cytotoxicity in A549 spheroids using the CellTiter-Blue® and CellTiter-Glo® cell viability assays, which assess metabolic activity (resazurin conversion) and adenosine triphosphate (ATP) levels (via luciferin conversion), respectively.[4,32,104] Other viability assays have also been used. These include the Perfecta3D® cell viability kit, which assesses enzymatic cleavage of the tetrazolium salt WST-1 to formazan by cellular mitochondrial dehydrogenases in viable cells,[4] and the acid phosphatase (APH) assay,[105,106] which measures activity of APH, an enzyme present in the cytosol of viable cells.[105] The trypan blue exclusion assay (also used to measure cell viability post-exposure), while useful for obtaining an initial count for a single-cell suspension, was not used due to the potential confounding effect of spheroid dissociation on cell viability.[103] Also commonly used are the MTT assay,[100] colorimetrically measuring the presence of oxidoreductase enzymes in viable cells, the Ki-67 tumour proliferation marker-staining assay,[97] as well as the xCELLigence™ impedance reader, analysing the growth of cells in real time.[101]

The Promega (Madison, WI, USA) CytoTox-ONE™ Homogeneous Membrane Integrity Assay[107] has also been employed to quantify cell viability by measuring resorufin (converted from resazurin) fluorescence coupled to release of lactate dehydrogenase (LDH) through compromised membranes of non-viable cells. This reaction in the form of a kit has been used in assessment of PCOOH-AuNP cytotoxicity with no interference.[82] This assay is particularly

suitable to spheroids, since unlike other viability assessments, cells do not need to be fixed to a surface or individually counted.[108,109] The LDH released into surrounding medium is quantified.[110]

1.5.2 Assay interference by PCOOH-AuNPs

Due to the fluorescence/absorbance of NPs, interference with certain assays is of some concern.[111] Possible cell viability assay interferences have been assessed and reported for the same formulation of PCOOH-AuNPs used in this study (Table 1.2).[112]

Table 1.2: Outcome of investigations into interference by gold nanoparticles in cytotoxicity and cell viability assays.[112]

Viability assay	Aspect affected by PCOOH-AuNPs
XTT assay	Optical interference of PCOOH-AuNPs with absorbance readings at 450 nm, absorption of both XTT substrate and formazan product.
LDH assay	No effect observed when reading the fluorescence of resorufin (resazurin conversion is coupled to LDH presence).
DCF assay	Quenching of DCF fluorescence.
PI dye	Quenching of PI fluorescence.

Abbreviations: XTT; 2,3-bis-(2-methoxy-4-nitro-5-sulfophenyl)-2H-tetrazolium-5-carboxanilide, LDH; lactate dehydrogenase, DCF; dichlorofluorescein, PI; propidium iodide.

Interference data were useful in subsequent selection of suitable assays. Ong *et al.*[111] have also detailed common examples of interference for silicon, cadmium, titanium, and zinc NPs, where the lactate dehydrogenase assays (LDH), alamarBlue™ Cell Viability Reagent (Invitrogen, Waltham, MA, USA), and tetrazolium-based assays such as MTT, 2,3-bis-(2-methoxy-4-nitro-5-sulfophenyl)-2H-tetrazolium-5-carboxanilide (XTT), and 3-(4,5-dimethylthiazol-2-yl)-5-(3-carboxymethoxyphenyl)-2-(4-sulfophenyl)-2H-tetrazolium (MTS) are frequent candidates for NP interference.[111] This has been corroborated by Kroll *et al*.[113] The PCOOH-AuNPs can bind to proteins and dyes, and possess their own optical properties such that indicator molecules and/or enzymes lose their function.[111] Thus, the selection of appropriate cytotoxicity assays is not only of great importance, but must also include a control for the possible interferential effect of the NPs in the selected assays. The determination thereof forms part of PCOOH-AuNP characterisation and assay optimisation.

Since no fluorometric PCOOH-AuNP interference has been observed for resorufin emission wavelengths in the LDH assay,[112] cytotoxicity assessments in this study were carried out using the LDH assay.

1.6 Rationale for use of an alveolar carcinoma cell line

In this study, the A549 alveolar carcinoma cell line (ATCC® number: CCL-185™) was selected for three principal reasons. First, comparability: NP uptake studies have been carried out recently in monolayer cultures of pulmonary origin (BEAS-2B bronchial epithelial cells).[50,82] Second, clinical relevance to inhalation drugs (using an alveolar cell line)[114] and occupational exposure to AuNPs, and third, the A549 cells' proven propensity for spheroid formation.[4,104,115,116]

The choice of lung tissue is partly due to relevance in the field of occupational health. Workers in mines are highly likely to be exposed, via inhalation and skin contact, to incidental nanomaterials. Characterisation of these NPs is extremely difficult, given their heterogeneity: varying size, shape, spectra, and chemical/physical properties.[117] However, without characterisation, exposure cannot be documented, effects of said exposure cannot be measured, and many workers' health remains at risk.[117] A contributor to this current problem is a lack of standardised sampling, indexing and measurement methodologies, leading to poor gauging of the extent and danger of incidental nanomaterial exposure.[117] This supports the interest of this study: developing an *in vivo*-representative *in vitro* NP testing platform, able to produce data on both cytotoxicity and cellular uptake, using an alveolar carcinoma cell line.[40,56-58]

The aforementioned nanomedicines (Section 1.3.2) mainly involve systemic administration for treatment of lung-related cancers, but the non-invasive nature of general inhaled aerosol drugs also qualifies this route of administration for therapeutic consideration in the context of nanomedicine.[118] Inhaled drugs avoid first-pass metabolism, are delivered directly to the disease site (if respiratory), and have a large amount of surface area available for both local activity and systemic absorption.[118] Inhalation (pulmonary) administration has been widely studied, especially in the field of nanomedicine.[118-120]

1.7 Aim, objectives, and study outline

This study aimed to establish a drug discovery and toxicity testing platform using A549 spheroids, for the elucidation of gold nanoparticle uptake mechanisms employed by these cells.

The objectives of the study (Fig. 1.6) were to:

1. Establish a reproducible A549 spheroid model with measurement of:
    a. Morphology using phase contrast and fluorescence microscopy
    b. Viability using the lactate dehydrogenase assay
2. Determine cytotoxicity of PCOOH-AuNPs in spheroids using the LDH assay
3. Assess uptake mechanisms employed by spheroids using applicable pharmacological inhibitors in combination with hyperspectral microscopy

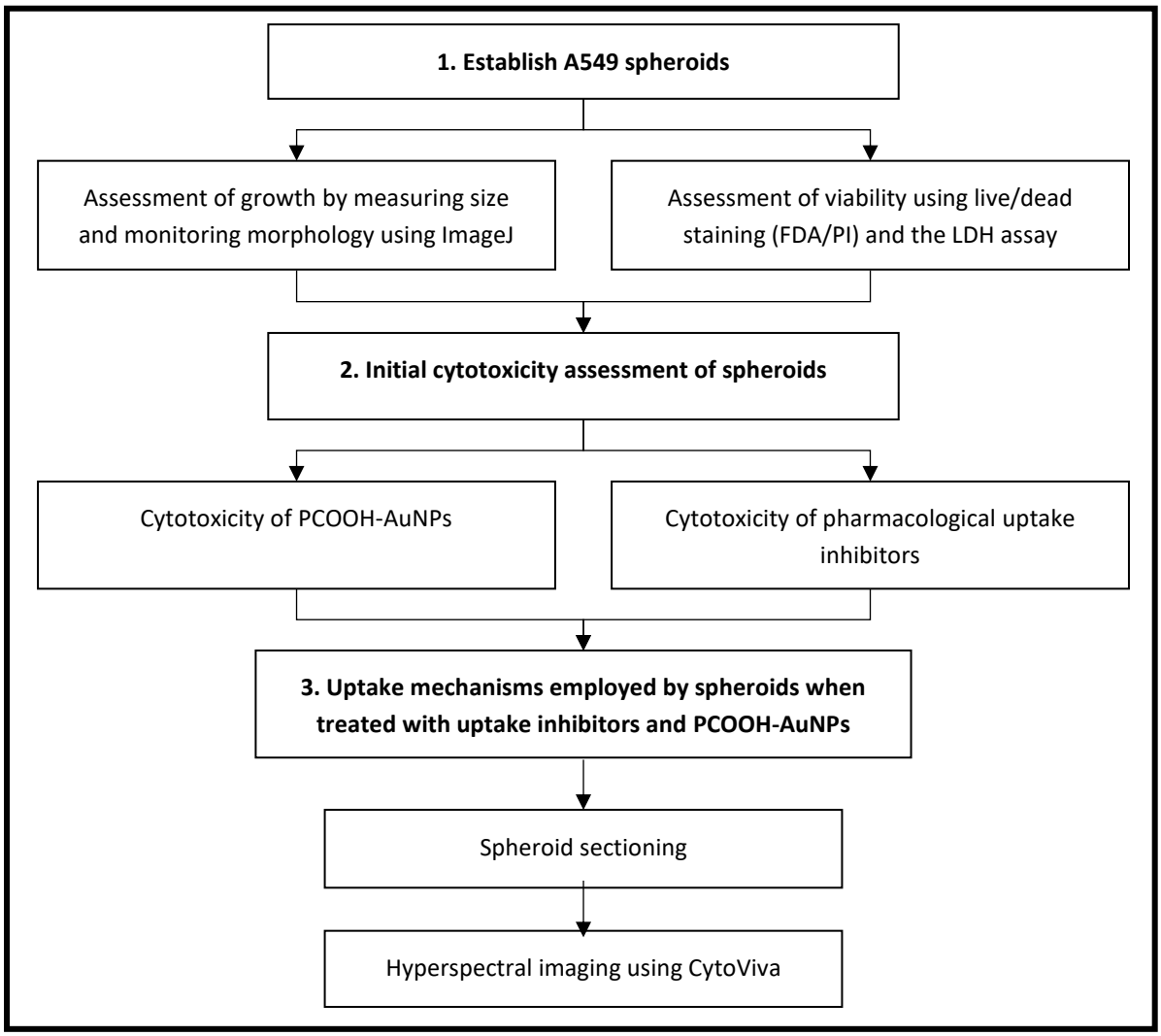

Fig. 1.6: Study outline.

Chapter 2: Materials and Methods

2.1 Ethical clearance

This project, and the entirety of the experimentation referred to herein, was approved (REC 540/2019) by the Research Ethics Committee of the University of Pretoria's Faculty of Health Sciences (Appendix I).

2.2 Materials

Reagents were procured and prepared as described in Appendix II.

2.3 Synthesis and characterisation of PCOOH-AuNPs

Gold nanoparticles were manufactured and functionalised by Mintek (Randburg, South Africa) as described by Vetten *et al.*[50] Negatively charged 14 nm citrate-capped AuNPs, as hosted by the Joint Research Centre (JRC) Nanomaterials Repository of the European Union,[50] were synthesised under sterile conditions using sodium citrate as a reducing agent. Attachment of PEG ligands was achieved by adding trisodium citrate to boiling tetrachloroaurate (both aqueous solutions) and boiling the solutions under reflux for 15 min. The suspension was cooled to room temperature and stirred overnight, then filtered through a 0.25 µm sterile syringe filter. The PCOOH-liganded AuNPs were prepared using ligand-exchange, to replace citrate groups, via saturation in PEG ligands with carboxyl functional groups.

Characterisation of PCOOH-AuNP physicochemical properties was also carried out by Mintek (Randburg, South Africa). Size and concentration of PCOOH-AuNPs were determined using an FEI Tecnai™ T12 TEM (ThermoFisher, Swedesboro, USA) at 120 kV. The PCOOH-AuNPs were placed on formvar-coated copper grids and dried, then measured using ImageJ (National Institutes of Health, USA). Absorbance spectra were measured preliminarily using a CECIL CE3021 spectrophotometer (Cecil Instruments, Cambridge, UK) at wavelengths from 400 to 800 nm. Charge, as zeta (ζ)-potential, was measured using a Zetasizer Nano ZS (Malvern Panalytical, Malvern, UK) at 25°C.

2.4 Assessment of nanoparticle interference

The PCOOH-AuNPs (stock solution: 4.1 nM) were diluted in either dH_2O or Gibco™ Dulbecco's Modified Eagle Medium (DMEM; Life Technologies Limited, Paisley, UK) to 1 nM to determine characteristics in different solutions. A volume of 100 µL pure PCOOH-AuNP suspension was measured spectrophotometrically from 200 to 800 nm to assess spectral activity, predictive of optical interference, using a Synergy II microplate reader (Biotek Instruments, Inc., Winooski, USA). Fluorescence emission and excitation characteristics were also measured using a Synergy II microplate reader for the filter set relevant to fluorometric readings in this study (excitation wavelength, emission wavelength [nm]): 485±40, 590±35. Additionally, possible PCOOH-AuNP interference, of both physical (quenching) and chemical (alterations to conversion) nature, was assessed with the LDH assay substrate (Promega CytoTox-ONE™ reagent [resazurin]) and fluorescent product (resorufin) at the above-mentioned wavelengths. Quenching was assessed by comparing the fluorescence intensity (FI) of equal volumes (100 µL) of resorufin in the presence and absence of PCOOH-AuNPs, while conversion was measured by incubating cell-free blanks (DMEM) containing PCOOH-AuNPs in the presence of Promega CytoTox-ONE™ reagent.

2.5 Maintenance of the A549 alveolar carcinoma cell line

The A549 alveolar carcinoma cells were cultured in 25 cm^2 cell culture flasks in DMEM containing phenol red as a pH indicator, supplemented with 10% heat-inactivated foetal calf serum (FCS) and 1% penicillin/streptomycin at 37°C in a humidified atmosphere of 5% CO_2. Medium was changed every 2 to 3 days as required.[114]

Once cell density had reached approximately 80% confluence, medium was decanted, and cells were washed with 0.1 M phosphate-buffered saline (PBS). Cells were chemically detached using TrypLE™ Express Enzyme for 3-5 min at 37°C in a humidified atmosphere of 5% CO_2 and centrifuged (200 *g* for 5 min) in FCS-supplemented medium. The pellet was resuspended in 1 mL FCS-supplemented medium, counted using the trypan blue exclusion assay (0.1% in PBS) and a haemocytometer, and diluted to the desired seeding density of 7.5 x 10^5 cells/mL.

2.6 Seeding and spheroid formation

The liquid overlay technique, as described by Senavirathna *et al*.,[106] was employed for spheroid generation of A549 cells in this study. To create a low-attachment surface, 75 µL of 1.6% low gelling temperature agarose solution was pipetted into clear, flat-bottom, 96-well plates, swirled to induce concavity, and allowed to solidify by cooling. The agarose solution was made up by first creating a 4% (w/v) agarose solution in PBS, then diluting it to 1.6% using FCS-free DMEM. The wells on the edges of the plate received 200 µL sterile PBS to reduce evaporation of medium from wells containing cells. Cells (100 µL, 7.5 x 10^4 cells/well) were seeded onto the agarose bed. Cells were incubated for 72 h to allow for formation, and the medium replaced via aspiration every three days thereafter. Spheroids were grown for a maximum of 21 days during optimisation.

2.7 Spheroid growth and viability

Spheroid growth and viability were assessed as described in Sections 2.7.1. to 2.7.3 at regular intervals (4, 7, 10, 14, 18, and 21 days), with Day 4 spheroids serving as baselines, due to no sooner investigation than after 72 h being possible.

2.7.1 Spheroid growth via microscopy

Morphological aspects of spheroids were evaluated using phase contrast microscopy and ImageJ (National Institutes of Health, USA).[121,122] Phase contrast microscopy is an optical technique allowing imaging of transparent specimens by converting the phase-shift of transmitted light to changes in brightness in the image.[121]

Morphological features,[123] such as circularity index and growth via spheroid diameter, were assessed via a Zeiss Axiovert 200M inverted microscope (Carl Zeiss, Inc., Oberkochen, Germany) and a 5X objective lens. The spheroid's circularity index, a parameter which indicates the degree of circularity on a scale from 0 (elongated polygon) to 1.0 (perfect circle) was measured with the below formula on ImageJ (automatically detecting spheroids' perimeters using contrast). Spheroid diameter and circularity indices were reported incrementally over 21 days.

$$Circularity = 4\pi \left(\frac{area}{perimeter^2}\right)$$

2.7.2 Spheroid viability via microscopy

Live/dead staining is an important tool used to confirm areas of viability and cell death within spheroids.[4] Fluorescein-diacetate (FDA) is the acetylated derivative of the green fluorescent compound, fluorescein.[124] Cell membranes are permeable to the acetylated, non-fluorescent FDA.[124] Internally, metabolically active cells hydrolyse FDA to fluorescein via esterases, which remains in the intracellular environment due to its charge.[108,124] Propidium iodide (PI) enters membrane-compromised cells and fluoresces red upon intercalation with nucleic acids; thus, membrane integrity can be inferred from PI exclusion.[108,125]

Spheroids were harvested and transferred to a 24-well plate after being washed thrice with PBS. In a dark room, 1 mL FDA/PI staining solution was added to each well. Excess staining solution was then removed by washing the spheroids thrice with 1 mL PBS for 1 min. Spheroids were imaged immediately using a Zeiss Axiovert 200M inverted microscope with filter sets for Texas red (for PI fluorescence) and fluorescein isothiocyanate (for FDA fluorescence), and a 5X objective lens. Images were processed and combined using ImageJ.

2.7.3 Spheroid growth via lactate dehydrogenase

The Promega CytoTox-ONE™ Homogeneous Membrane Integrity Assay[107] (Madison, WI, USA) was employed to quantify cell growth, whereby released LDH was measured in an assay coupled to the conversion of resazurin to resorufin.[110] Lysing all cells in each well enables measurement of LDH released into a defined volume of medium, which is proportional to number of cells present.

At Days 4, 7, 10, 14, 18 and 21, with microscopic selection ensuring proper formation and consistent morphology and size, spheroids were transferred to opaque-walled 96-well plates. All medium was aspirated, then replaced with 50 µL of medium containing 1 µL (equivalent to 2% [v/v]) CytoTox-ONE™ Lysis Solution, then incubated for 5 min at room temperature (~22°C). Cell-free blanks were included for removal of background noise. A volume of 50 µL CytoTox-ONE™ reagent was then added to each well. The plates were shaken for 1 min, incubated for 10 min at room temperature, and FI was read immediately thereafter at emission/excitation (±bandpass filter range) wavelengths (nm) of 485±40/590±35,

respectively. All values were blank-subtracted, averaged and expressed as a percentage of growth at Day 4, using the equation (*y* denoting number of days since day 4):

$$FI\ (\%\ growth\ relative\ to\ Day\ 4) = \frac{Average\ FI(Day\ [y])}{Average\ FI(Day\ 4)} \times 100$$

2.8 Assessment of cytotoxicity in spheroids

The Promega CytoTox-ONE™ Homogeneous Membrane Integrity Assay, as described in Section 2.7.3, was used to assess cytotoxic effects of PCOOH-AuNPs and pharmacological inhibitors on the A549 spheroids.

Cytotoxicity testing was performed on Day 7 spheroids. All medium was aspirated from spheroids and replaced with 50 µL DMEM alone (negative control) or supplemented with 0.4% (v/v) DMSO (vehicle control), 2.0% (v/v) CytoTox-ONE™ lysis solution (positive lysis control), 1 nM PCOOH-AuNP or pharmacological inhibitor (concentrations stated in Table 2.1). Spheroids were exposed for 2 h and 24 h for PCOOH-AuNPs alone, and for 3 h for pharmacological inhibitors (a period exceeding that of literature-based time needed to inhibit uptake systems). The 2 h exposure period was used for comparison to previous studies,[50] and the 3 h exposure period was used to account for the necessary pre-treatment time during the inhibition assay. The LDH release was compared to the Day 7 negative control. A blank consisting of 50 µL DMEM only was used to control for background noise.

Table 2.1: Inhibitory concentration ranges for pharmacological inhibitors' cytotoxicity assessment.

Inhibitor	Concentration used	Reference
Sodium azide	10 mM	Zhu *et al.*[126]
Dynasore	80 µM	Macia *et al.*,[127] Zhu *et al.*[126]
EIPA	25 µM	Han *et al.*,[93] Commisso *et al.*[128]
Genistein	200 µM	Vetten *et al.*[50]
Chlorpromazine	14 µM	Vetten *et al.*[50]

Abbreviations: EIPA; 5-(N-ethyl-N-isopropyl) amiloride.

2.9 Elucidation of cellular uptake mechanism(s) used by spheroids for nanoparticle uptake

2.9.1 Incubation with pharmacological inhibitors and PCOOH-AuNPs for uptake inhibition assay

Inhibitory concentrations of each pharmacological inhibitor were used to elucidate the uptake mechanism employed by cells for PCOOH-AuNPs, following specific treatment regimens (Fig. 2.1).

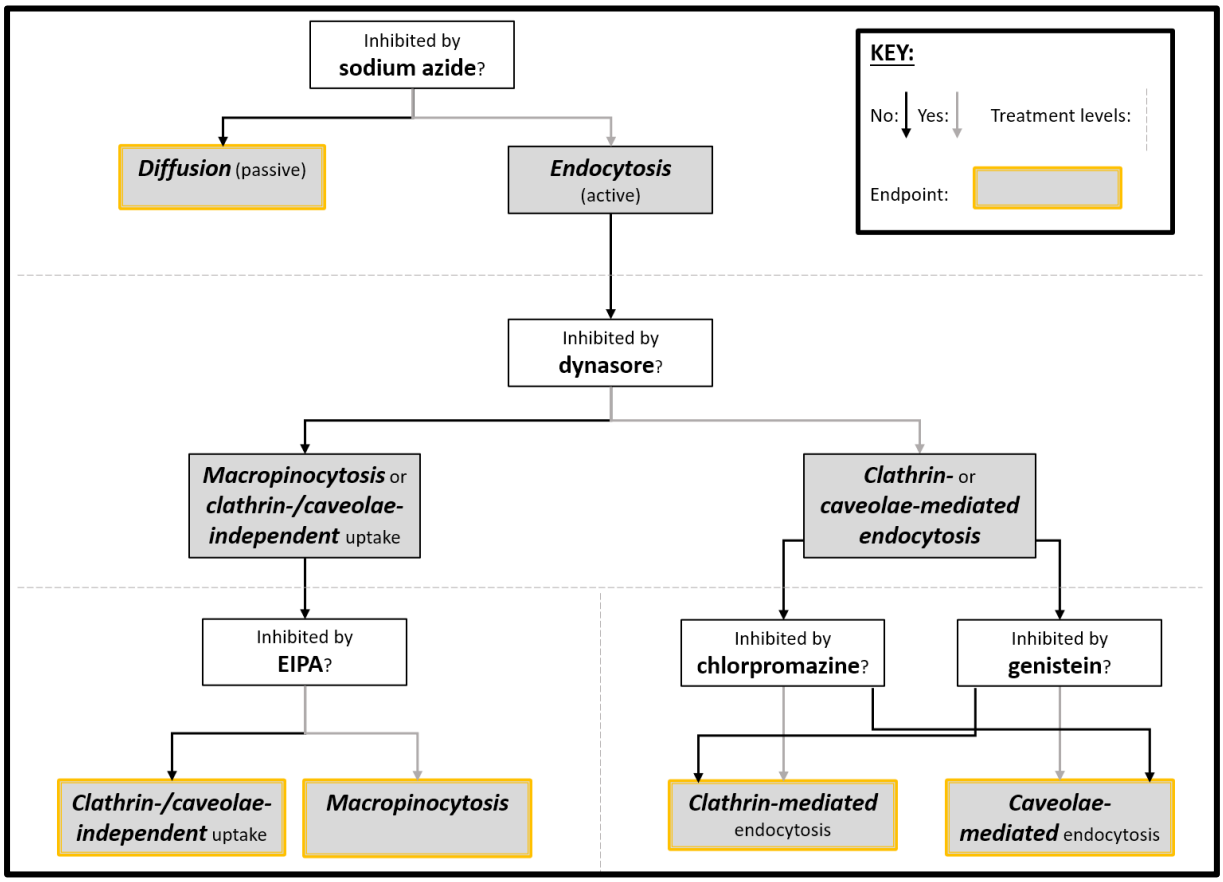

Fig. 2.1: Dichotomous key showing the selection process of pharmacological Inhibitors in uptake mechanism elucidation. The flow diagram is to be read from the top down, and uptake was assessed after each dichotomous operator. Abbreviations: EIPA; 5-(N-ethyl-N-isopropyl) amiloride.

In previous studies carried out by collaborators of this study, cells were exposed to PCOOH-AuNPs for varying times; namely, 1, 4, and 6 h,[82] as well as 2 and 5 h periods.[50] Similar exposure intervals were considered for this research; however, for two reasons were not carried out. Firstly, a study using the same PCOOH-AuNPs and a related (BEAS-2B) cell line succeeded the above collaborator's study.[82] Exposures of 2 h were deemed sufficient as there

were minimal changes in intracellular levels of PCOOH-AuNPs compared to 1 h exposures.[82] Indeed, even 24 h incubations at five-fold higher concentrations showed no uptake change in cells initially resistant to NP uptake in the former study.[50] Secondly, in both of the above studies, differences in cell lines[82] and differences in functionalisation[50] were being investigated, necessitating such parameters. As a baseline, where uptake could be expected in cells capable of such, 2 h exposure has proven suitable.

Spheroids' medium was completely removed by aspiration and replaced with 100 µL DMEM alone or supplemented with pharmacological inhibitors (concentrations as per Table 2.1) or 0.4% (v/v) DMSO (vehicle control) for 1 h at 37°C. Thereafter, 33 µL of PCOOH-AuNP stock solution was added to each well to achieve a final concentration of 1 nM, and incubated for a further 2 h at 37°C, as carried out by Vetten *et al.*[50] An additional 24 h exposure time-point was included for the uninhibited PCOOH-AuNP sample alone to assess long-term uptake.

2.9.2 Sectioning of spheroids for analysis

Spheroids were sectioned by aspirating all media from spheroids representing each treatment class, then placing them onto an aluminium grid. Lone spheroids were then immersed in Tissue-Tek® O.C.T Compound (Sakura Finetek, Torrance, CA, USA) matrix and frozen at -30°C. Sections (5 µm) were made using a Shandon Cryotome E (Thermo Scientific, Waltham, MA, USA) as per the CytoViva® User manual.[94] Sections were fixed directly to standard glass slides in dried Tissue-Tek® for storage (at room temperature) and microscopy.

2.9.3 Hyperspectral imaging using CytoViva®

Hyperspectral scans of the sectioned spheroids were generated using ENVI 4.8 software and the CytoViva® hyperspectral imaging (HSI) system (CytoViva, Inc., Auburn, USA) available at the NIOH. High-resolution illumination microscopy system (CytoViva, Inc., Auburn, USA) was used to assess intracellular uptake, calculated by counting PCOOH-AuNPs present intracellularly in a defined area.[101] Prior to scanning of sections, the particle filter feature was used to create spectral libraries for the PCOOH-AuNPs present within spheroid sections of the uninhibited control, as detailed in the method by Roth *et al*.[129] This spectral library was used in conjunction with spectral angle mapping (SAM) to match pixels from the spectral image obtained to the corresponding pixels from the optical image obtained of the PCOOH-AuNP-

treated cells using microscopy. Particle presence was thereby confirmed. Dark-field images were viewed at 60X magnification using the CytoViva® 150 Unit in conjunction with an Olympus BX43 microscope and a Dagexcel X16 camera. ImageJ was then used to obtain counts of PCOOH-AuNPs taken up (within a constant region of interest of fixed area [A]). Data obtained in this way were used as semi-quantitative measures of PCOOH-AuNP uptake, for comparison of uptake in cells exposed to PCOOH-AuNPs in the absence and presence of pharmacological inhibitors. Nanoparticle uptake was calculated as a percentage of the uninhibited control using the equation:

$$\frac{NP}{A}\,(\%\,relative\ to\ uninhibited\ positive\ control) = \frac{Average\ \frac{NP}{A}(inhibited\ experiment)}{Average\ \frac{NP}{A}(uninhibited\ positive\ control)} \times 100$$

2.10 Statistical analyses

Statistical analyses were carried out using Microsoft® Excel® and GraphPad Prism® 5. All data were expressed as mean ± standard error with at least three biological and three technical repeats. Statistical significance was set at *p* values < 0.05. Comparisons to the negative control were made using a Kruskal-Wallis test with post-hoc Dunn's test.

Chapter 3: Results

3.1 Ensuring gold nanoparticle specifications

Upon manufacturing, PCOOH-AuNPs were characterised by Mintek. Methods used were able to define size, concentration, UV absorbance maxima and surface charge (Table 3.1). The PCOOH-AuNPs have a slightly positive surface charge and are 14 nm in size, with low variation.

Table 3.1: Post-synthesis nanoparticle characterisation

Characterisation	Result
Size ± variance	14 ± 2 nm
Concentration	4.1 nM; equivalent to 2.5 x 10^{12} NPs/mL
UV absorbance maximum	523 nm
Surface charge (ζ-potential)	+0.972 mV

Abbreviations: ζ; zeta, NPs; nanoparticles.

Spectral and fluorometric mapping of PCOOH-AuNPs revealed spectral activity at 520 nm when suspended in dH_2O (Fig. 3.1A), which shifts to 560 nm when suspended in growth medium (Fig. 3.1B). Negligible fluorometric activity (Fig. 3.2) was observed when considering the minimal scale of autofluorescent activity shown by the NPs.

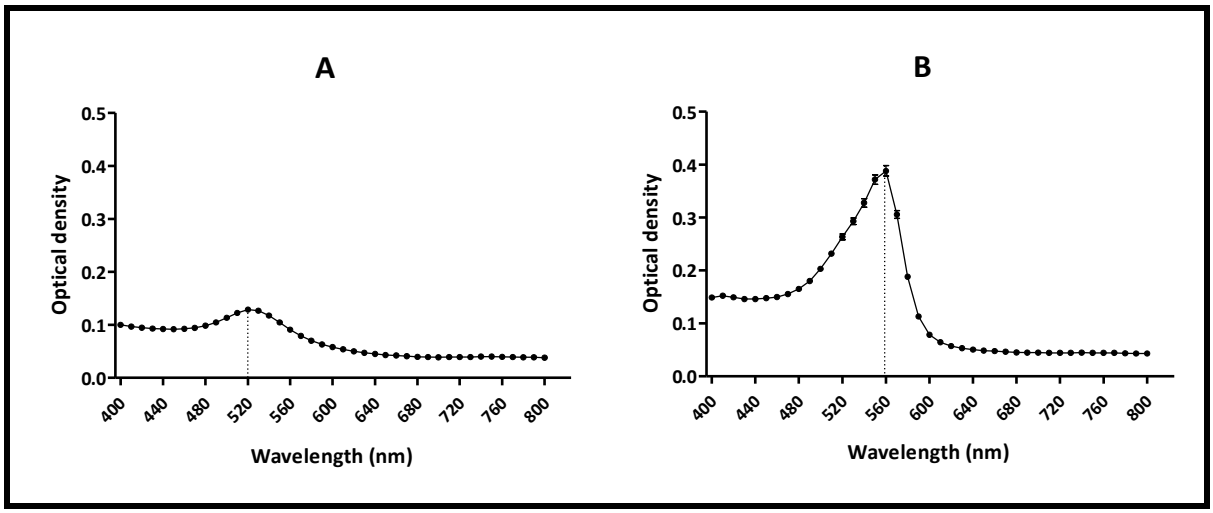

Fig. 3.1: Spectral mapping of 1 nM PCOOH-AuNPs in dH_2O (A) FCS-supplemented DMEM (B). Abbreviations: PCOOH-AuNP; carboxyl polyethylene glycol-functionalised gold nanoparticle, DMEM; Dulbecco's Modified Eagle Medium.

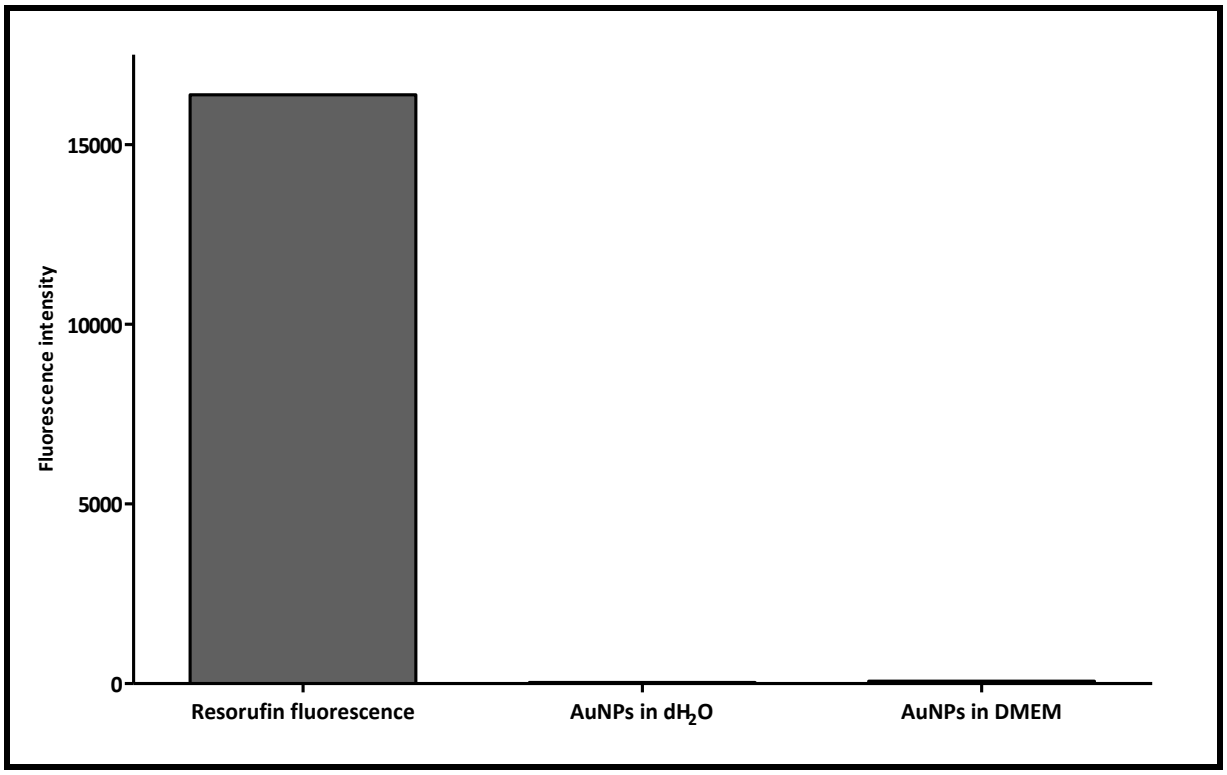

Fig. 3.2: Fluorometric mapping of 1 nM PCOOH-AuNPs in dH_2O and FCS-supplemented DMEM. Resorufin, at experimental intensity, has been shown for scale. The 485±40, 590±35 filter set (nm; excitation, emission wavelengths ± bandpass filter ranges) was used for generation of this graph. Abbreviations: PCOOH-AuNP; carboxy polyethylene glycol-functionalised gold nanoparticle, dH_2O; Distilled water, DMEM; Dulbecco's Modified Eagle Medium.

Interference assessment of the PCOOH-AuNPs revealed non-significant ($p > 0.05$) quenching (Fig. 3.3A) of resorufin fluorescence by 5.26% relative to an PCOOH-AuNP-free sample. Comparison of 1 nM PCOOH-AuNP (in DMEM) cell-free blanks to those containing only DMEM, resulted in a 0.6% increase in conversion (Fig. 3.3B) of non-fluorescent resazurin (substrate) to fluorescent resorufin (product).

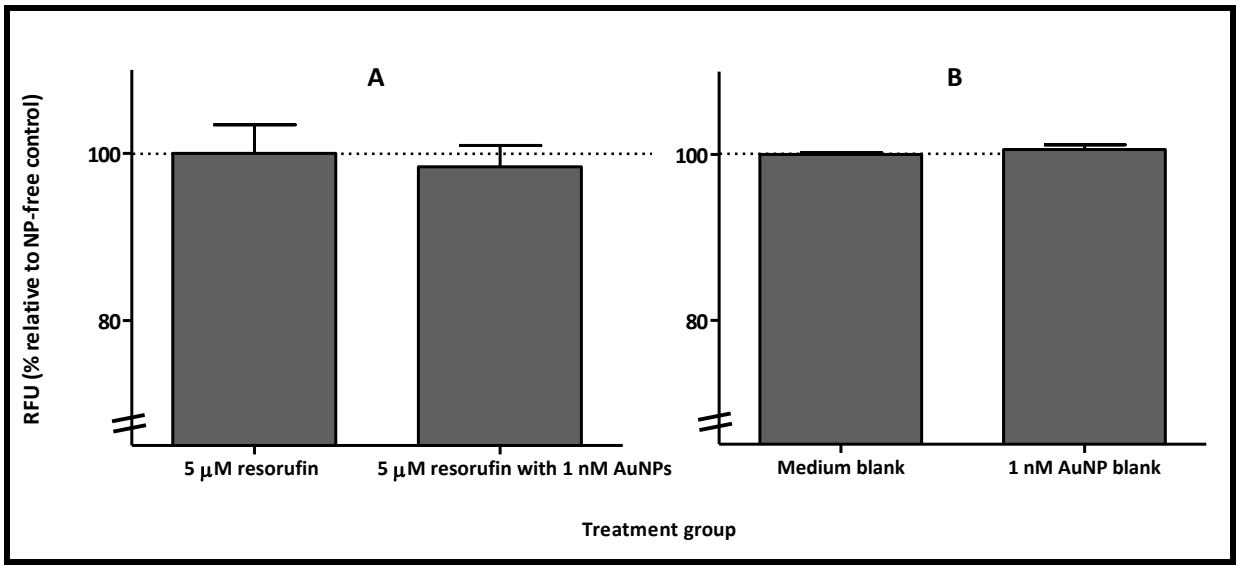

Fig. 3.3: Nanoparticle interference with the LDH assay, in terms of quenching of resorufin fluorescence (A) and non-fluorescent substrate conversion in the absence of cells (B). Abbreviations: AuNP; gold nanoparticle, RFU; relative fluorescence units.

3.2 Spheroid morphology and growth

3.2.1 Morphology

Spheroids gradually increased in both diameter and circularity within the first 10 days since seeding (Fig. 3.4). Thereafter, circularity levels decreased as spheroids began to lose structural integrity. Diameter changes also correlated with spheroid growth; however, beyond day 14, this metric became falsely inflated due to uniform loss of structural integrity. This was evident from the increase in variability in both metrics beyond Day 14. At Day 7, an average diameter and circularity index of 702.11 ± 10.77 µm and 0.80 ± 0.03, respectively, were observed. Day 7 spheroids were used for further experimentation as they allowed for an appropriate experimental window for assays to be conducted thereafter, remaining stable for around three more days thereafter. As is evident in Fig. 3.4, Day 7, Day 10 and Day 14 spheroids showed circularity indices of 0.7974, 0.8534, and 0.8054, respectively. Although these remained within 5% of one another, stability was appropriate from Day 7 until Day 10, then began to decline.

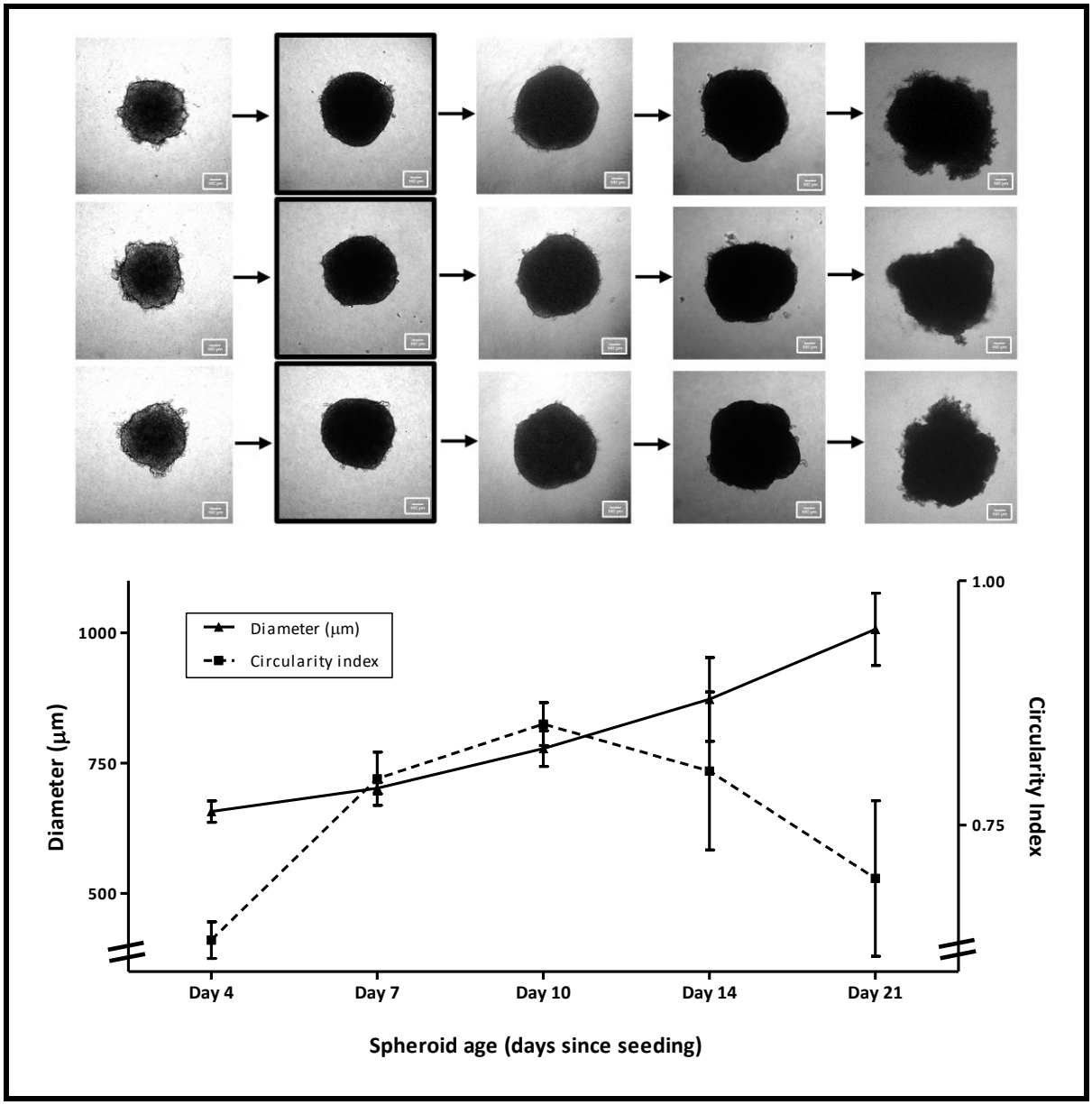

Fig. 3.4: Visual and numerical representation of morphological changes in A549 Spheroids over time. Outlined are the spheroids at Day 7, when they were considered appropriate for use in all assays within in this study. Spheroids shown here are representative images captured over the course of experimentation. Scale bar = 100 µm.

3.2.2 Spheroid growth

Spheroid growth was steady, but plateaued approaching Day 21. The LDH released upon lysis of spheroids increased uniformly (r^2 = 0.9833) from Day 4 onwards, however, displayed high variation – a caveat of 3D *in vitro* techniques requiring high levels of manipulation (Fig. 3.5).

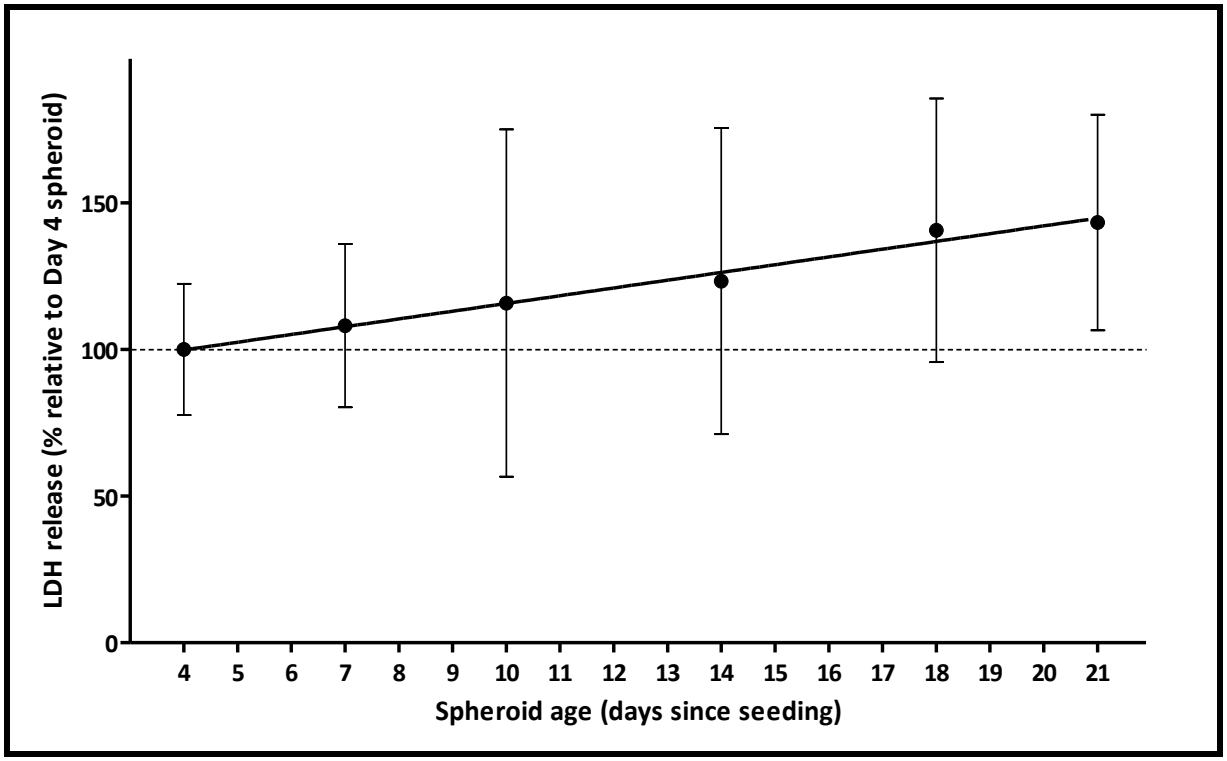

Fig. 3.5: Growth of spheroids over time, expressed as a percentage relative to Day 4 spheroids. Growth depicted by line of best fit. Measured by lysing all cells within a spheroid and quantifying cell numbers proportional to LDH release.

3.2.3 Live/dead staining

Live/dead staining indicated zones of viability and cell death (Fig. 3.6). Fluorescein fluorescence was higher towards the outer layer of the spheroid, but steadily decreased towards the core of the spheroid. The PI fluorescence was partially distributed throughout the spheroid; however, staining was centralised to the spheroid's core.

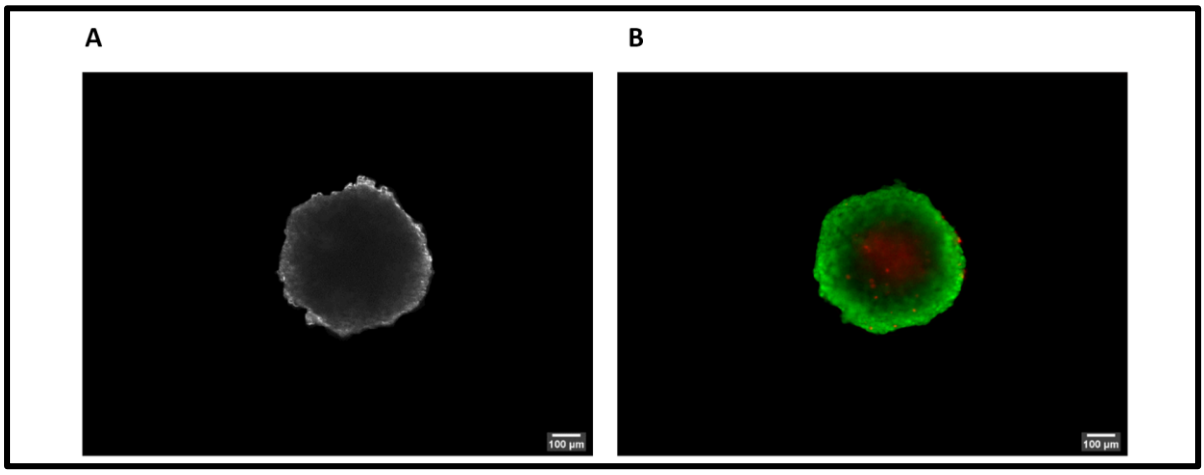

Fig. 3.6: Live/dead staining using FDA/PI. Phase contrast image (A) and stained image (B). These pictures differentiate between zones of metabolic activity (green) and areas compromised cell membranes (red).

3.3 Cytotoxicity assessment of spheroids

3.3.1 Gold nanoparticles

The presence of PCOOH-AuNPs with spheroids did not result in an increase in LDH release compared to the negative control. The PCOOH-AuNPs reduced LDH activity (non-significantly [$p > 0.05$]) by 3.1 and 3.7%, after 2 and 24 h exposures, respectively. Thus, no cytotoxicity was noted in the A549 spheroids over 24 h exposure to the PCOOH-AuNPs (Fig. 3.7A).

3.3.2 Pharmacological uptake inhibitors

Pharmacological uptake inhibitors showed no cytotoxicity in Day 7 spheroids after 3 h exposure to inhibitory concentrations thereof (obtained from literature – Table 2.1). The LDH release was not increased compared to the negative control (Fig. 3.7B).

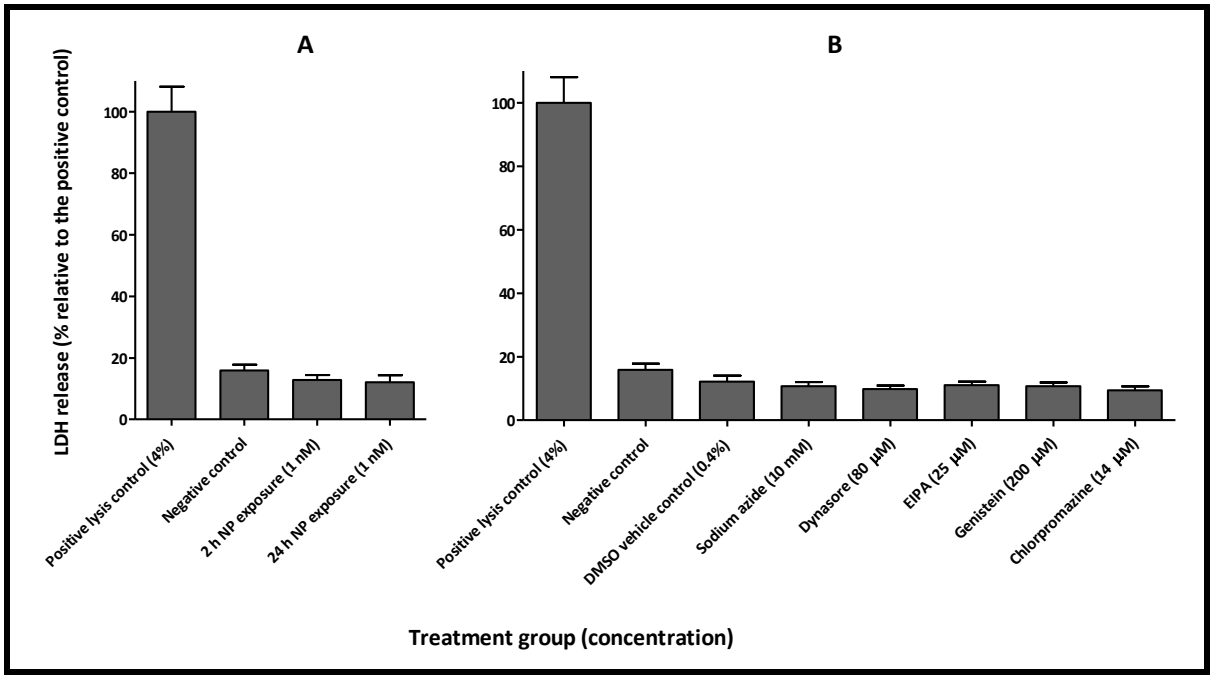

Fig. 3.7: Lack of cytotoxicity after 2 and 24 h exposures to AuNP (A) and pharmacological inhibitors' 3 h exposure (B). Abbreviations: AuNPs; gold nanoparticles, EIPA; 5-(N-ethyl-N-isopropyl) amiloride.

3.4 Spectral angle mapping of internalised PCOOH-AuNPs

Spectral angle mapping of internalised PCOOH-AuNPs using the CytoViva® HSI scanner showed spectral peaks at ~600 nm. These NP spectra were detected from internalised PCOOH-AuNPs within 5 µm spheroid slices of the 24 h uninhibited control group. Spectra of endocytosed PCOOH-AuNPs with (Fig. 3.8A) and without (Fig. 3.8B) background spectra (due

to cell spectra) were generated. The process of subtracting background noise ensures that in later detection, using CytoViva®, mapped PCOOH-AuNP spectra are not due to anything other than PCOOH-AuNPs.

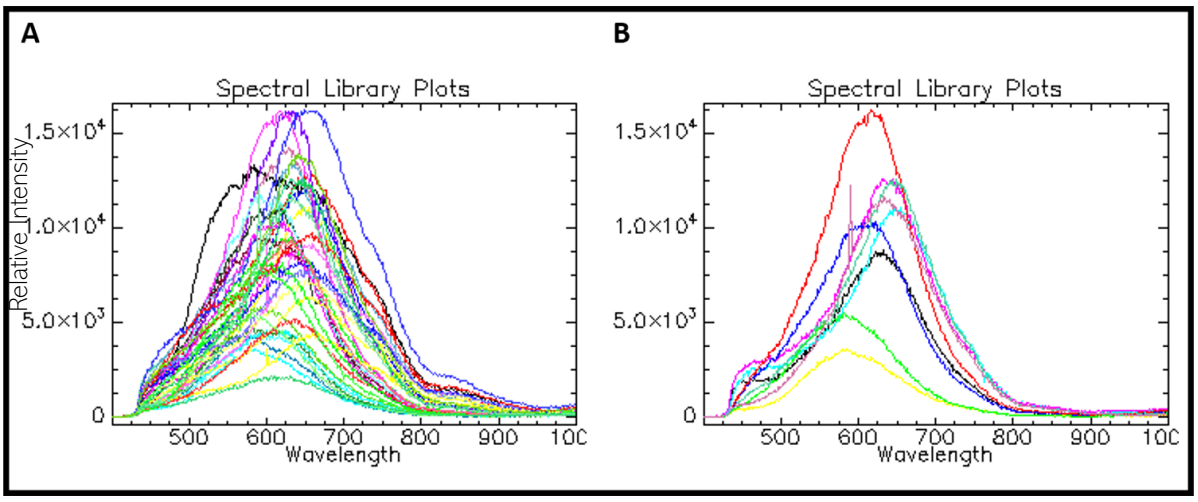

Fig. 3.8: Spectral Library Plots resulting from a hyperspectral scan of endocytosed gold nanoparticles within cells. (A) All spectral activity included; (B) spectra after subtracting negative control as cellular background.[129]

Obtaining an endocytosed NP count involves a three-step process. First, a hyperspectral scan is captured in the form of an HSI (Fig. 3.9A). Second, spectra detected as those belonging to PCOOH-AuNPs are mapped onto the scan (Fig. 3.9B), and third; mapped PCOOH-AuNPs within a region of interest of constant area (Fig. 3.9C) are counted. Three types of images are thus generated (Fig. 3.10), each with a particular purpose.

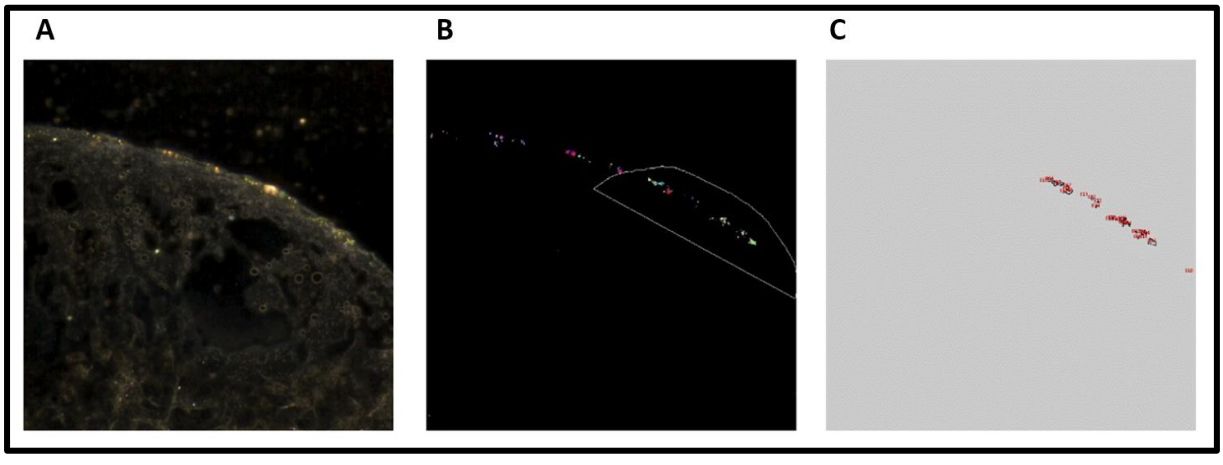

Fig. 3.9: Representative 60X hyperspectral scan (A), SAM image with region of interest (B), and processed counting image (C), of a 24 h PCOOH-AuNP-treated, uninhibited control captured using CytoViva®. Abbreviations: SAM; spectral angle mapping.

Representative HSI scans from each treatment class (Fig. 3.10) indicated the accumulation of PCOOH-AuNPs on the periphery of the spheroid. Low regional NP uptake was evident, with penetration of NPs not exceeding 4.5 µm from the spheroid edge. Penetration deeper towards the cores of spheroids was poor, and it was observed in the CytoViva® images that even cells exposed to PCOOH-AuNPs for 24 h did not show an increase in NP penetration into the spheroid, when compared to that of the 2 h exposure group. Background noise, as mentioned, is visible in Fig. 3.10 (A) and (D), and has been excluded from analysis.

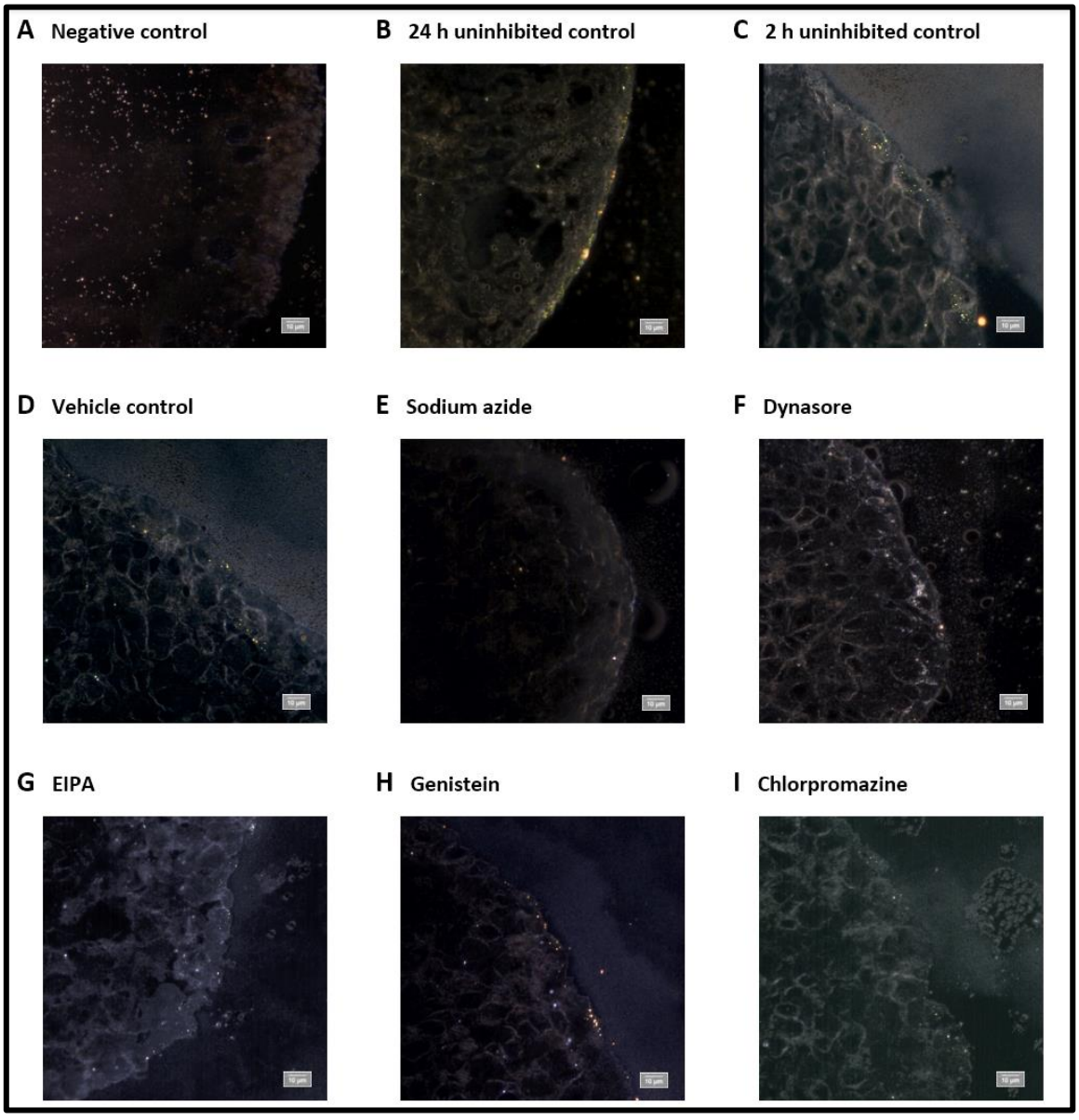

Fig. 3.10: Representative 60X hyperspectral images captured using CytoViva®. What appears to be fluorescent activity in (A) and (D) is due to light reflecting off immersion oil on samples. All activity in NP-free samples was not mapped by the CytoViva® system, and was thus discounted as interference. Abbreviations: EIPA; 5-(N-ethyl-N-isopropyl) amiloride.

3.5 Nanoparticle counts

Using SAM and ImageJ, PCOOH-AuNP counts were obtained for each treatment class (Fig. 3.11A). Inhibited uptake never exceeded that of the 2 h uninhibited control, showing that intended inhibition was achieved. Comparison between the 2 h and 24 h exposures revealed a non-significant ($p > 0.05$) increase by 18.1 NPs/area in uptake for the 24 h incubation (Fig. 3.11B). The vehicle control showed a non-significant ($p > 0.05$) increase in uptake by 2.2 NPs/area. Other AuNP counts per area reductions observed with comparison to the 2 h uninhibited control included sodium azide (21.4 NPs/area; $p < 0.0001$), dynasore (15.8 NPs/area; $p < 0.05$), EIPA (1.5 NPs/area; $p > 0.05$), genistein (0.7 NPs/area; $p > 0.05$), and chlorpromazine (7.9 NPs/area; $p > 0.05$).

Using NP/area counts, proportions of endocytic mechanisms employed may be calculated (Fig. 3.12), based on the widely agreed-upon[61,62,69] understandings thereof (Fig. 1.4). The 2 h uninhibited control (Fig. 3.12A) was considered the 100% uptake benchmark treatment group. Observations and calculations are presented in table format (Table 3.2) and proportions of uptake as parts of a whole, with reference to the dichotomous inhibitor tree, in chart format (Fig. 3.13). Observable in these results is an overlap in employment of clathrin- and caveolae-mediated endocytosis.

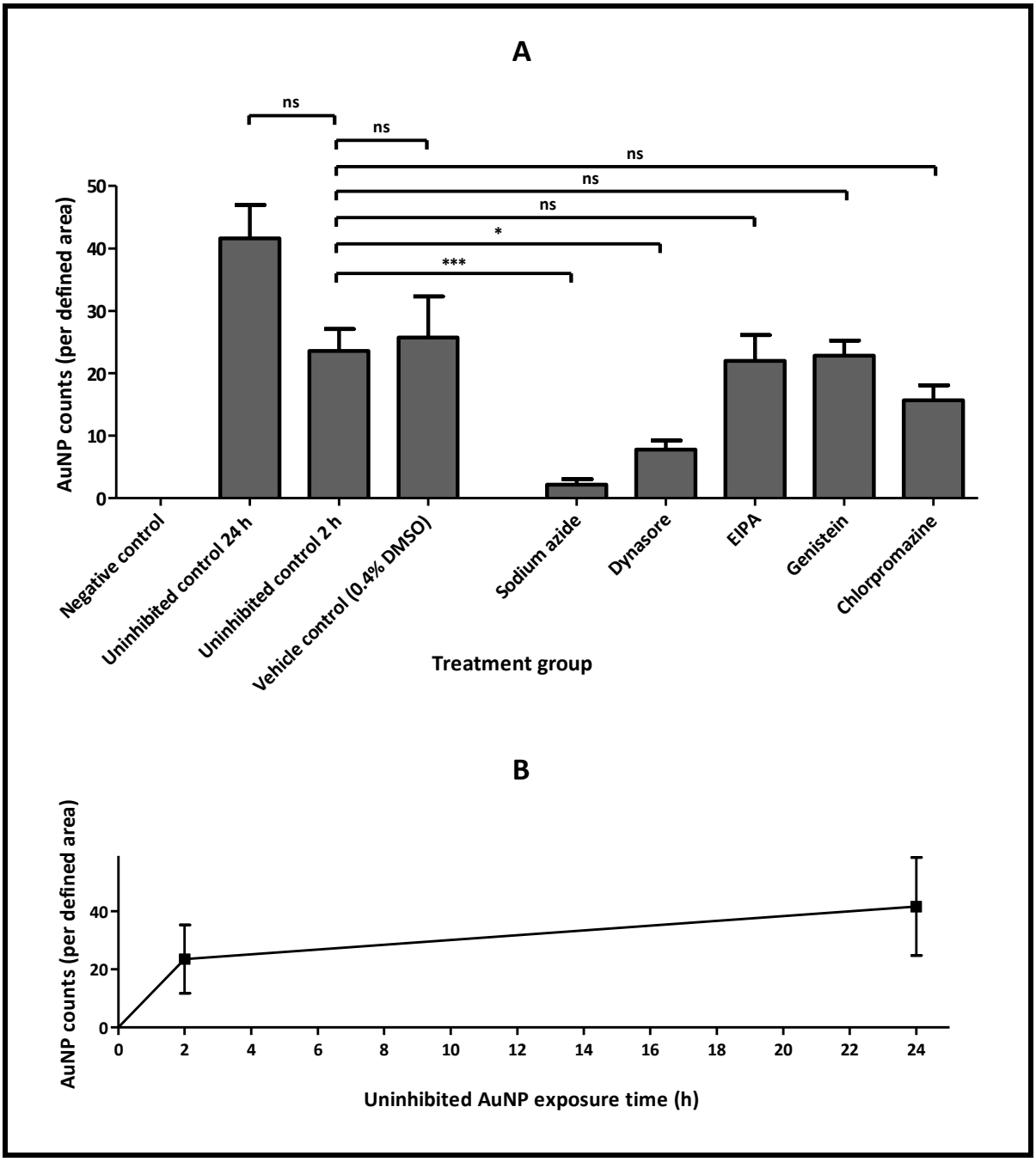

*Fig. 3.11: Internalised gold nanoparticle counts per defined area, assessed by CytoViva®. Total counts for each treatment group (A) and the increase in uptake over time (B) are shown. Abbreviations: DMSO; dimethyl sulfoxide, EIPA; 5-(N-ethyl-N-isopropyl) amiloride, ns; non-significant. * $p < 0.05$, *** $p < 0.0001$.*

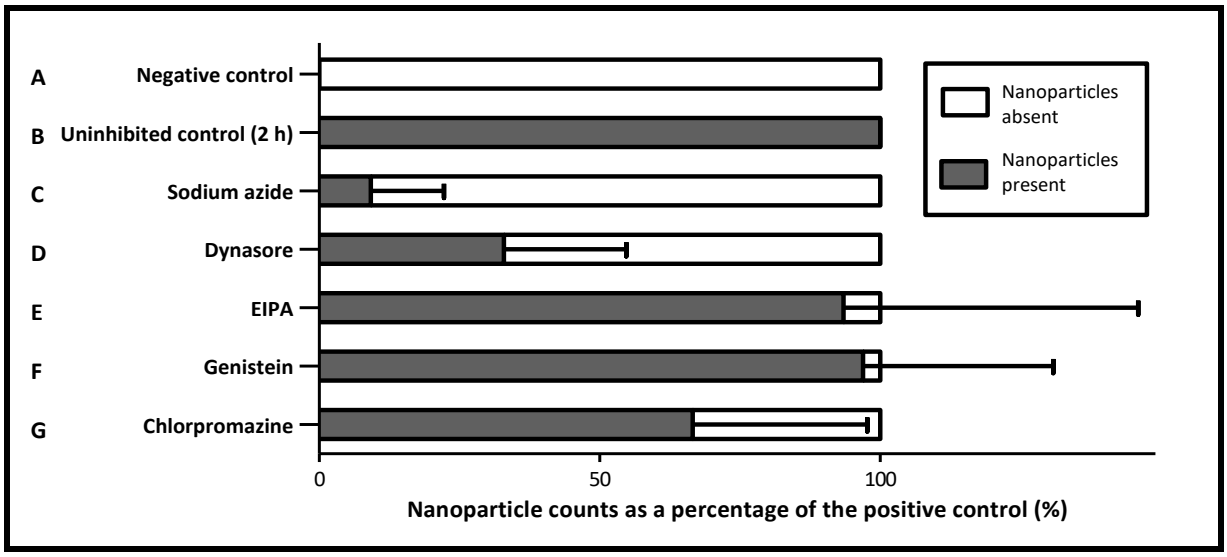

Fig. 3.12: Internalised nanoparticle counts as a percentage of the uninhibited control. Abbreviations: EIPA; 5-(N-ethyl-N-isopropyl) amiloride.

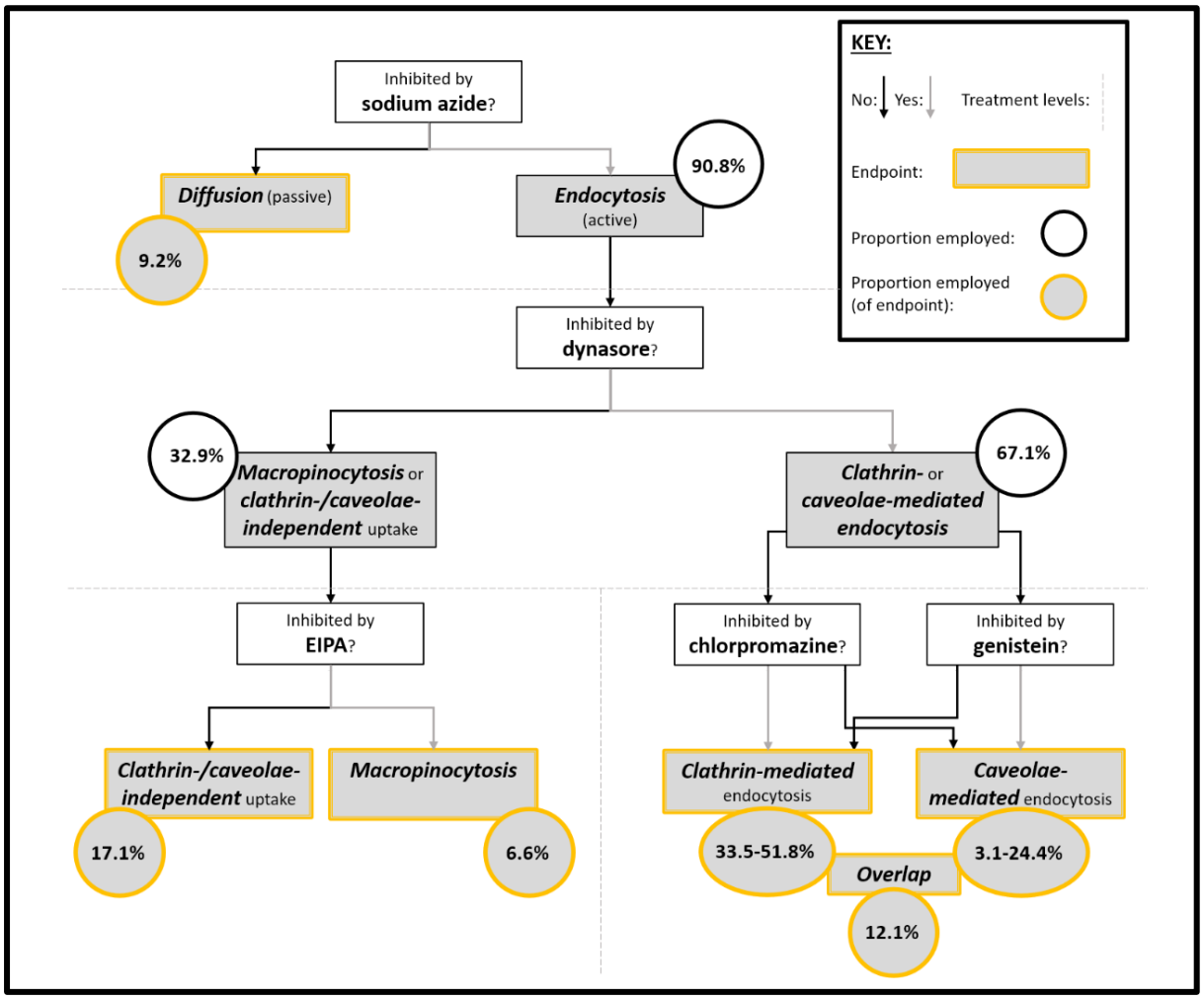

Fig. 3.13: Dichotomous key (as in Fig. 2.1) depicting inhibitor selection and pathway deduction, with added uptake mechanism proportions (rounded to the nearest decimal. Ranges are given for clathrin- and caveolae-mediated endocytosis). Abbreviations: EIPA; 5-(N-ethyl-N-isopropyl) amiloride.

Table 3.2: Observations, calculations, and results of employed uptake mechanisms by A549 spheroids for gold nanoparticles.

Treatment (Fig.)	Observations	Calculations	Conclusions
Sodium azide (3.12B)	90.8% of uptake inhibited	$[Total\ uptake] - [Sodium\ azide\ inhibition] = [uptake\ due\ to\ passive\ diffusion]$ $\therefore 100.0\% - 90.8\% = 9.2\%$	**9.2%** of uptake is due to passive diffusion.
Dynasore (3.12C)	67.1% of uptake inhibited	$[Total\ uptake] - [Dynasore\ inhibition] = [uptake\ due\ to\ dynamin\ independent\ processes]$ $\therefore 100.0\% - 67.1\% = 32.9\%$	**67.1%** of uptake is due to dynamin-dependent processes (clathrin- and caveolae-mediated endocytosis). **32.9%** of uptake is due to macropinocytosis, clathrin- and caveolae-independent uptake, or passive diffusion.
EIPA (3.12D)	6.6% of uptake inhibited	$[Dynamin\ independent\ processes] - [passive\ diffusion] - [macropinocytosis] = [uptake\ due\ to\ clathrin\ and\ caveolae\ independent\ proces$ $\therefore 32.9\% - 9.2\% - 6.6\% = 17.1\%$	**6.6%** of uptake is due to macropinocytosis. **17.1%** of uptake is due to clathrin- and caveolae-independent processes.
Genistein (3.12E)	3.1% of uptake inhibited	$[Caveolin\ independent\ processes] - [passive\ diffusion] - [dynamin\ independent\ processes] = [maximum\ uptake\ due\ to\ clathrin\ mediated\ endocytosis\ upon\ caveolin\ inhibition]$ $\therefore 96.9\% - 9.2\% - 32.9\% = 54.8\%$	**96.9%** of all uptake is due to mechanisms other than caveolae-mediated endocytosis. Caveolae-mediated endocytosis accounts for min. **3.1%** of all uptake. Clathrin-mediated endocytosis accounts for max. **54.8%.**
Chlorpromazine (3.12F)	33.5% of uptake inhibited	$[Clathrin\ independent\ processes] - [passive\ diffusion] - [dynamin\ independent\ processes] = [maximum\ uptake\ due\ to\ caveolae\ mediated\ endocytosis\ upon\ caveolin\ inhibition]$ $\therefore 66.5\% - 9.2\% - 32.9\% = 24.4\%$	**66.5%** of all uptake is due to mechanisms other than clathrin-mediated endocytosis. Clathrin-mediated endocytosis accounts for min. **33.5%** of all uptake. Caveolae-mediated endocytosis accounts for max. **24.4%.**

Abbreviations: EIPA; 5-(N-ethyl-N-isopropyl) amiloride, max; maximum, min; minimum.

Chapter 4: Discussion

4.1 Spheroid formation and growth

4.1.1 Formation

Spheroids generated over the course of this study were approximately 702 µm in diameter on Day 7. With maturation over 21 days, an increase in diameter was gradually offset by a decrease in circularity from Day 10 onwards. This suggests a loss of structural integrity after Day 10. For the purposes of the experimental requirements, Day 7 was deemed morphologically appropriate due to i) viability, ii) diffusion properties, and iii) time-to-use.[4,21,22] At Day 7, spheroids were compact, with defined edges and high circularity. Zones of viability were characteristic of liquid overlay-generated spheroids, with high metabolic activity in more superficial layers. Spheroids > 1 000 µm tend to have larger zones of cell death[22] as a result of poor diffusion of oxygen and other small molecules (up to 200 µm in size); depriving cells of essential nutrients.[21] This is similar to what has been noted in *in vivo* avascular solid tumours.[21] Optimisation phases of this study also revealed flattening, and poor morphology and compaction in larger spheroids (Appendix III), which was remedied with small tweaks to methodology, and greater care to allow spheroids to remain completely still within the days immediately following seeding.

In order to achieve higher diffusion of nutrients and waste, porous scaffold-based 3D-culture methods would have become necessary.[22] As mentioned, scaffold-free methods were sufficient for the nature of data generated in this study. Lastly, as noted by Cui *et al.*, an economical method of spheroid formation within a short timeframe should be of paramount importance in selection of spheroiding methods.[21] As a result of both the anti-adhesive surface, and the tendency for adherent cells to aggregate,[21] the A549 spheroids formed compact structures. Cadherins accumulate extracellularly and bind to homophilic cadherins on adjacent cells, causing cellular compaction, more accurately mimicking the *in vivo* milieu.[22] Spheroids grow while compacting and maturing, but only to an extent: as the liquid overlay model does not continuously remove metabolic waste or provide a perfused system for nutrient delivery, the longevity thereof is limited. However, scaffold-free methods prove efficient and economical; thus, further aligning studies based thereupon to global

objectives.[21] These include universally enhancing reproducibility and overall quality of 3D (and other) *in vitro* methods and the drug discovery pipeline.[9,21]

Spheroids remained stably formed for the period between Days 7 and 10, allowing for assays, exposures and other spheroid-based experiments to be conducted within a feasible timeframe when begun on Day 7. This culture period was sufficient for the purposes of the current experimental setting. From Day 14 onwards, spheroids became less structurally stable, showing an increase in diameter accompanied by a decrease in circularity. If the spheroids were to be maintained in culture for periods exceeding 21 days, a more efficient means of nutrient exchange, as well as structural support are required, to avoid a build-up of waste and increased hypoxia.[22] Scaffold-based techniques, bioreactors and co-culturing methods have been able to achieve longer growth.[22,34,130] However, it is agreed-upon[131,132] that spheroids larger than 500 µm in diameter, displaying zonation, closely resemble the cellular morphological differentiation of *in vivo* solid tumours.[4] Thus, the spheroiding method in this study has proven capable of producing meaningful results as a NP testing platform in 3D cultures within a feasible timeline. Furthermore, while many spheroiding techniques have not proven capable of producing large (> 500 µm) spheroids,[4] the liquid overlay technique has been capable of doing so reproducibly.

4.1.2 Growth and viability

According to the ATCC, the doubling time of monolayer A549 alveolar carcinoma cells is 22 h.[114] The slower growth seen once cells are grown in 3D is supported by Zanoni *et al.*, who noted that the presence of ECM reduces growth signalling, and slows the growth rate of aggregated 3D cultures.[4] Spheroids form at different rates depending on the cell line and culture conditions,[32] rendering comparative literature review to be merely a guide as to what might be expected. Variability is relatively high for the cell growth data: a small caveat arising out of the inherent variation present in *in vitro* spheroid formation.

Live/dead staining uses FDA/PI to visualise growth of and morphological zonation within spheroids,[108] however, it is not capable of standalone viability assessment.[125] As such, live/dead images were considered alongside spheroid growth data via LDH release. High outer fluorescein fluorescence indicates more viable, metabolically active cells, with higher

potential for proliferation.[4] The PI fluorescence, indicative of compromised cell membranes and dead cells, appears higher closer to the core of the spheroid (Fig. 3.6), though there is some distribution thereof. Distribution of small areas of cell death is to be expected, as regions of the spheroid may shift out of formation and die.[4,115] The superficial layers of spheroids possess cells that adhere only loosely to the main central structure. Lower fluorescein levels on the inside of the spheroids indicate lower metabolic activity, which is due to lower availability of nutrients and O_2, as well as a higher incidence of quiescent cells.[4,88] This observation is corroborated by the spheroid growth curve which appears to decrease, as well as the visible diminishing of structural integrity of the spheroids with age; however, given variability, will require additional experimentation to generate more definitive data.

4.2 Cytotoxicity studies

The two-fold purpose of the cytotoxicity assays in this study was to further characterise the effects of the selected PCOOH-AuNPs on the spheroids, and to confirm that pharmacological uptake inhibitors, at concentrations recommended in literature,[50,93,126-128] were not cytotoxic. Since neither the inhibitors nor the PCOOH-AuNPs caused an increase in LDH release from spheroids compared to the negative control, no cytotoxic effect was observed. This is supported by Vetten *et al.,*[50] where six types of AuNPs of similar size and varying functionalisations, including PCOOH, were assessed, and not one of them showed any cytotoxicity compared to an untreated negative control in the BEAS-2B bronchial epithelial cell line.[50] This speaks to the inert state of these AuNPs, no matter the functionalisation, as well as potential for application in drug delivery mechanisms under similar conditions found in this study.[50]

Mechanisms of, and reasons for cytotoxicity are explored in studies focusing thereupon. Findings in this study are supported by Tlotleng *et al.*, where 14 nm PCOOH-functionalised AuNPs, over the same exposure time of 2 h, were not toxic in either the HepG2 hepatocellular carcinoma or the HEK 239 human embryonic kidney cell lines.[101] Other assessments of PCOOH-functionalised AuNPs have confirmed the same in the Cos-1 *Cercopithecus aethiops* kidney cell line,[133] as well as the BEAS-2B bronchial epithelium cell line.[50]

Pharmacological uptake inhibitors are required to be non-cytotoxic to avoid confoundment of uptake assessment.[82] As such, an appropriate concentration within inhibitory ranges (Table 2.1) was assessed for each inhibitor.

4.3 In-suspension PCOOH-AuNP mapping and SAM of internalised PCOOH-AuNPs

The PCOOH-AuNPs may undergo changes in the presence of serum proteins, or have been taken up by cells: their hydrodynamic diameters increase and/or protein coronas form.[74,87] These changes bring about size fluctuations in the PCOOH-AuNPs, which alter their absorbance spectra.[134] The results of spectral mapping of the PCOOH-AuNPs in Section 3.1 support the expected change in hydrodynamic diameter of the PCOOH-AuNPs when in contact with serum proteins.

In a similar way, prior to SAM image acquisition using CytoViva®, particles needing to be detected intracellularly must be scanned such that, by presence of wavelengths in scanned cellular material, their presence can be confirmed. However, spectral activity of cellular material itself can later generate a large amount of spectral background noise, leading to the potential for false PCOOH-AuNP detection.[129] Thus, to enhance the accuracy and resolution of this system, spectra not due to PCOOH-AuNPs captured from the negative control (considered background noise) were subtracted from the spectral plot, in a manner described by Roth *et al.*[129] The noise-reduced spectral library generated was used for the detection of PCOOH-AuNPs throughout all CytoViva® imaging and SAM image acquisition.

4.4 Gross PCOOH-AuNP uptake into A549 spheroids

In this study, gross PCOOH-AuNP uptake was low at approximately two PCOOH-AuNPs per cell, even after 24 h incubation (Fig. 3.10). A previous investigation by collaborators into 14 nm citrate-capped AuNP uptake into BEAS-2B monolayer cultures indicated up to ~100 AuNPs being internalised per cell over a 4 h incubation.[82] In their case, the difference in uptake was not affected by AuNP functionalisation. This was evident in a subsequent study,[50] where the same PCOOH-AuNPs showed higher levels of uptake than the aforementioned citrate-capped AuNPs.[82] In the monolayer culture method, it is surmised that all cells are equally exposed to

NPs. In the case of a spheroid, AuNP penetration efficiency and transcytosis come into play. PCOOH-AuNPs were only observed in superficial layers of the spheroids in this study. Research carried out in monolayers[9,50] may thus provide confounded results as monolayers are exposed equally with no multilayer transport required, reaffirming their inability to sufficiently represent or translate to the *in vivo* research environment.[15]

Behzadi *et al.* found that although NPs are internalised by various means, if they are not trans- or exocytosed, or secreted from the cytoplasm, the NPs remain in the intracellular environment, or are trafficked to the lysosome.[71] Further to this, the microenvironment surrounding a spheroid, including the presence of ECM, pH alterations, and fluctuating nutrient levels, all affect NP uptake and intracellular destinations.[135] The microenvironment is capable of altering NP properties and protein adsorption,[136] thereby affecting interactions with cell membranes and decreasing uptake – this is necessary to consider when studying NPs.[71,135]

4.5 Uptake mechanisms employed and intracellular trafficking of PCOOH-AuNPs

The use of CytoViva®[82,129] in this study did not allow for definitive detection of subcellular localisation, however, desirably allowed for a label-free approach, non-destructive sample preparation, and a wide range of suitable sample-embedding matrices.

The intracellular destination of endocytosed particles may be deduced by perusing literature reporting the intracellular fate of cargo taken up by a respective mechanism. Employed uptake mechanisms observed in this study were discussed here, alongside expected intracellular trafficking pathways, noting how mechanism employment is affected by cell type, NP type, and NP characteristics (Table 4.1).

Table 4.1: Retrospective study predictive of likely intracellular localisation following specific endocytic processes and proportions thereof employed in this study (Fig. 3.13).

Mechanism of uptake	Percentage employed	Expected subcellular destination	Reference
Phagocytosis	0.0%	Lysosome	Conner *et al.*[61]
Passive diffusion	9.2%	Unspecified, cytosol	Rothen-Rutishauser *et al.* [67]
Macropinocytosis	6.6%	Macropinosome	Conner *et al.*[61]
Clathrin- and caveolae-independent endocytosis	17.1%	Endosome, lysosome, cytoplasm, and recycling endosome	Mayor[73] and Behzadi *et al.*[71]
Clathrin-mediated endocytosis	33.5% (min) 54.8% (max)	Endosome and lysosome	Kiss[137]
Caveolae-mediated endocytosis	3.1% (min) 24.4% (max)	Caveosome and endosome	Conner *et al.*[61]

Phagocytosis, which is well documented to favour a degradative fate in the low-pH environment of the lysosome, is not employed by A549 cells.[61] This is only carried out by immunological cells such as macrophages and monocytes and its effects were not considered in this study.[138]

Only a small percentage (9.2%) of PCOOH-AuNPs entered the cells via diffusion. This may be due to partial membrane damage or non-viable cells near the spheroid's surface.[125] The observed diffusion may also be due in part to the weak positive surface charge on the PCOOH-AuNPs in this study, rendering them very close to being neutral.[139] Studies have shown that neutral NPs show lower adsorption of surrounding serum proteins.[139,140] Decreased protein adsorption results in NPs retaining their lower hydrodynamic diameter;[74] thus, enabling more passive diffusion to take place.[67] A small amount of passive uptake occurring was corroborated by an uptake study in erythrocytes and NPs, where no cellular machinery exists other than a plasma membrane – an ideal platform for assessment of passive diffusion.[67,87]

Macropinocytosis, due to its bulk engulfment of surrounding material, lacks selectivity in the solutions and suspensions taken up,[141] supporting its low employment of 6.6% observed in this study. Macropinocytosis is of greater importance in the uptake of larger (average of 200 nm) NPs, but does not exclude smaller NPs found in suspension near the cell surface,

especially if agglomeration has taken place, increasing the NPs' hydrodynamic diameter to a size more likely to enter cells via macropinocytosis.[71,136] Additionally, trafficking of material taken up by macropinocytosis is largely dependent on the internalised substance, making it difficult to hypothesise intracellular trafficking post-macropinocytosis.[141]

Clathrin- and caveolae-independent endocytic pathways are typically poorly characterised.[61] In the present study they collectively allowed for 17.1% of uptake. It is believed that particles and other molecules taken up in this way assimilate into other trafficking pathways, making them relatively untargeted at a subcellular level.[62] These flotillin-, RhoA-, Cdc-42-, Arf1- and Arf6-mediated pathways are able to fuse with endosomes, so can also lead to a degradative fate in the late endosome or lysosome, or allow LMP to be induced.[69] As an example, one of the few known candidates for clathrin- and caveolae-independent endocytosis is folate.[71] Studies have found that folate and folate-bound molecules or particles, once bound to the folate receptor, are taken up conservatively and trafficked into the cytoplasm[142] or endosomes,[71,143] without degradation.[71] As such, especially in targeting of folate-demanding cancerous cells, folate-conjugation has become an attractive avenue in drug targeting.[71]

Clathrin-mediated endocytosis, responsible for between 33.5% and 54.8% of NP uptake in the present study, directs internalised cargo to either endosomes, degradative lysosomes, or towards the plasma membrane.[71,139] In the case of spheroids and *in vivo* tissues, a lysosomal endpoint may not be desirable, because once within a lysosome, particles may be trapped and prevented from exerting action, unless conjugated to a drug activated by enzymes or low pH there present.[35,71] In some cases, lysosomal trafficking may be desired as a means to bring about LMP, which can lead to mitochondrial membrane damage, autophagy, and cell death.[144,145] LMP induction has become a common target for NP-mediated cell killing.[145] However, findings suggest that LMP may only take place over longer periods of NP exposure: for example, following treatment with polystyrene NPs, populations of cells with damaged lysosomal membranes appeared after 1 h, but did not increase in number for 7 h thereafter.[144] Only after 24 h incubation was an increase noted.[146] When considering NPs as drug carriers, once within lysosomes, drugs or molecules may also degraded before activity is exerted.[139] This is problematic if the desired effect is not one mediated by the NPs themselves; thus, for this purpose, clathrin-mediated endocytosis should be avoided. The process of

clathrin-mediated endocytosis can take place in a receptor-independent manner, via non-specific electrostatic and hydrophobic interactions.[71] This renders it a widely-applicable mechanism of uptake.[71] The fate of an endocytosed substrate is often dependent on cargo-specific interactions with intracellular trafficking machinery after internalising.[141] The above findings relating to clathrin-mediated endocytosis employment, are widely supported by literature. Ding *et al.* has found that in the presence of FCS, 15 nm AuNPs are endocytosed primarily by clathrin-mediated endocytosis.[136] Further, the cationic charge of the PCOOH-AuNPs in this study suggests that they are more thoroughly endocytosed than anionic nanomaterials,[147] due to partiality towards clathrin-mediated endocytosis, as well as increased plasma membrane-NP interaction, increasing not only the extent, but also the rate thereof.[139,148] Though the PCOOH-AuNPs in this study are relatively weakly cationic, in an *in vivo* study by Elci *et al.*, AuNPs of a neutral or negative charge were taken up into lung tissue 8- and 10-fold less (respectively) than those carrying a positive charge.[149] Finally, it is worth noting that different cell lines employ different mechanisms of uptake for similar AuNPs.[50] Vetten *et al.* reported that caveolae-mediated endocytosis was the primary mechanism of uptake for similar AuNPs as used in this study into related bronchial epithelial cells (BEAS-2B).[50] Pathways concluding in lysosomal degradation are not favourable when considering AuNPs. Balfourier *et al.* studied the intracellular degradation of AuNPs, and noted that it begins with oxidase-mediated ROS induction within the lysosome.[150] The AuNPs then remain in the cells in the form of nanoleaves, which follow a similar degradation pathway to ionic gold.[150] Smaller (4 nm) AuNPs were degraded at a higher rate than larger AuNPs of the same type.[150]

Caveolae-mediated endocytosis, accounting for between 3.1% and 24.4% of NP uptake into spheroids, leads to internalised particles being trafficked temporarily to caveosomes and/or endosomes at neutral pH; thus, avoiding degradative fate in the lysosome.[71,137] Subcellular trafficking is generally accepted to be towards the smooth ER and Golgi complex.[137] This is the most desirable pathway when considering drug delivery or therapeutics,[55] as the taken-up substance either remains in the intracellular environment, cytosolically or within endosomes, or is trafficked through trans- or exocytosis to deeper layers of cells or tissue.[71,151] Particles may be functionalised via ligands for targeting to caveolae, such that degradation is

avoided.[139] When taken up in this way, better therapeutic and toxicity profiles are achieved, due to a targeted approach avoiding degradation.[139,152] However, it is difficult to achieve caveolae-mediated endocytosis, because unlike clathrin-mediated endocytosis, internalisation through caveolae requires specific activation by complex signalling pathways.[151] Agents responsible for upregulation are able to cause phosphorylation or dephosphorylation of membrane-bound receptors, and as such, caveolae-mediated endocytosis is very dependent on its endocytic cargo for direction of trafficking.[137] Indeed, given that trafficking from caveosomes to endosomes could result in degradative pathways, some few caveolae-endocytosed particles are also degraded in the lysosome.[61,137]

4.6 Pathway overlap

A potential mechanism employment percentage overlap of 12.1% exists between clathrin-mediated and caveolae-mediated endocytosis. Two potential reasons for this observation were investigated.

4.6.1 Uptake mechanism efficiency

Rates of endocytic pathways could play a role in the observed overlap, by allowing more uptake to occur more rapidly via one endocytic pathway than another.[153] Because of the relatively short incubation time employed in this study, the rate at which endocytosis occurs may play a confounding role, as in investigations by Rejman *et al.*[153] Using known ligands for clathrin- and caveolae-mediated endocytosis, it was observed that during the first 30 min of uptake, clathrin-mediated endocytosis occurred at more than double the rate of caveolae-mediated endocytosis.[153] The cumulative extent and endocytic rate of the two mechanisms become more comparable, and are nearly equal after 3 h.[153] This is supported by the fact that cationic NPs are widely regarded to be rapidly endocytosed via clathrin-mediated endocytosis.[148,149] Thus, when considering the above results and NP exposure time of 2 h, it is possible that the employment of clathrin-mediated endocytosis may be inflated compared to that of caveolae-mediated endocytosis.

4.6.2 Alternate endocytic pathway employment following inhibition

The observed overlap in uptake mechanisms may imply that a functionality overlap exists between clathrin- and caveolae-mediated endocytosis, given their similarities.[62] Overlapping

functionality, by virtue of a lack of depth of understanding of endocytic pathways,[35,71] is plausible; however, given the general rapidly adaptative nature of cancerous cells,[154,155] secondary activation is also worth investigation.

Endocytic pathways and endosomal trafficking are extremely dynamic pathways, as their response to stimuli differs based on the needs of a cell.[156] Similar to the current study, Dos Santos *et al.* observed this phenomenon.[157] Their study, carried out in three representative cell lines (including A549 cells) found that multiple pathways could be employed by a single cell line, for endocytosis of the same NPs, upon inhibition of a particular pathway.[157] However, the lack of definitive inhibition by pharmacological inhibitors does provide a challenge when attempting to draw conclusions from data generated.[157]

A study by Medina-Kauwe corroborates the above, further noting that altered endocytic mechanisms may be valuable drug delivery avenues.[158] Directing the uptake and intracellular trafficking of potential drugs presents the possibility of delivering active ingredients to specific intracellular compartments.[158] This has been achieved by numerous pathogens;[159-163] the best defined being the simian virus 40 (SV40).[158,159] The non-enveloped DNA virus, SV40, is able to utilise caveolae-mediated endocytosis by binding two specific receptors (one of which is found within a characteristic caveolae lipid raft), and thereby avoid degradation in the lysosome, which would otherwise ensue.[158]

4.7 Gold nanoparticle penetration and intercellular trafficking

The penetration of NPs into the cores of spheroids was, in this study, relatively low. From measurements made, it is unlikely that NPs were able to be trafficked more than one cell layer deep. This indicates low levels of transcytosis and diffusion, as well as high intracellular retention of PCOOH-AuNPs following endocytosis. This is due in part to the PCOOH-AuNPs' slightly positive charge: not only do neutral NPs show a higher percentage of diffusion, they are capable of greater penetration.[147] Thus, the PCOOH-AuNPs in this study, possessing a slightly positive surface charge, are expected to show poor penetration via passive routes. Regarding NP size, Perrault *et al.* reports that smaller AuNPs (sizes tested: 20-100 nm) tend to show better penetration into vasculature than larger ones.[139,164] However, NPs larger than 20 nm (40-100 nm) showed no statistically significant ($p > 0.05$) difference between each

other, and it was observed that the 20 nm NPs were able to move through interstitial space.[164] Movement through interstitial space is not emulated in this spheroid model, because of the relative simplicity, lack of varying cell types and deposition of ECM present.[22,33] For this reason, the discussion is led away from NP characteristics and onto spheroidal cell-based responses to the NPs.

Penetration of particles through a spheroid is also a function of the employed uptake mechanism. Caveolae-mediated endocytosis is known to have the potential to lead to transcytosis.[71] Therefore, the finding that it is not primarily employed in this study is corroborated by penetration, transcytosis, and intercellular trafficking being poor.[71] Tailoring NPs to trigger caveolae-mediated endocytosis has potential to increase transcytosis; thus, penetration into spheroids.[151] An exemplary application of this knowledge is described by Gradishar, in reference to the drug Abraxane®.[152] Abraxane® is an FDA-approved serum albumin-functionalised modification of paclitaxel, resulting in an improved therapeutic index.[139,152] This functionalisation enables caveolae-mediated endocytosis, followed by intercellular trafficking (via transcytosis) deep into solid tumours.[139,152]

It has been noted that tumour (spheroid) permeability and compaction play a key role in NP penetration.[139,165] Poorly permeable tumours were largely unaffected by therapy with a drug and nanocarrier, except in the case of 30 nm NPs.[165] Additionally, since highly permeable tumours in the same experiment yielded a greater degree of treatment efficacy, consistency and reproducibility of the spheroid model are of utmost importance when gathering uptake data. [165]

Chapter 5: Conclusion

5.1 Concluding remarks

The global drug discovery pipeline is in need of improvement, for example, through representative *in vitro* research platforms and better candidate drugs to be tested. Many issues arise out of a poor understanding of what occurs at the cell-environment interface. During this study, an advanced cell culture model of the A549 cell line was established to assess PCOOH-AuNP uptake. Spheroids were grown to an appropriate and reproducible size and density within seven days, and as such, allowed for a platform to be developed for various *in vivo* representative analyses. Additionally, the PCOOH-AuNPs investigated were, at 1 nM, not cytotoxic to the A549 alveolar carcinoma cell line in spheroid culture.

Hyperspectral imaging of internalised PCOOH-AuNPs revealed clathrin-mediated endocytosis to be the primary uptake mechanism employed for these NPs. This is undesirable, given its degradative subcellular destination, but there are advantages to clathrin-mediated uptake, such as the efficiency thereof and lack of requirement of a specific receptor. Caveolae-mediated endocytosis, responsible for the second-highest amount of endocytosis, is much more desirable for NPs, especially when regarding mechanisms of drug delivery and desirable applications thereof. The ability to target cargo towards being trafficked deeper into a solid tumour proves an elusive, but desirable characteristic.

Given the results, a model was successfully developed for the investigation of PCOOH-AuNP uptake into 3D A549 alveolar carcinoma spheroids using label-free means. Although the PCOOH-AuNPs themselves did not permeate deeply into the spheroid, evidence of their ability to do so exists, and informs future design of more tailored and efficacious AuNPs.

5.2 Study limitations

5.2.1 Specificity of pharmacological uptake inhibitors

Inhibition assays present in this study have been criticised for their specificity, exerting certain effects outside of their expected scope.[62] Instances of this include the following: Dynasore, a dynamin (GTPase) inhibitor, could reduce cholesterol in the plasma membrane, thereby affecting caveolae-mediated and clathrin- and caveolae-independent endocytosis.[166] Cell line discrepancies may also be present, Rejman *et al.* finding that extent of uptake inhibition by chlorpromazine and genistein may be dependent on the cell line used.[153]

Inhibition assays also tend to lack highly specific, reliable positive controls.[157] This was overcome using uninhibited and untreated controls. An alternative to inhibition is RNA transcriptome interference at loci encoding proteins essential to certain pathways.[166] However, most methods utilising gene silencing techniques are poorly characterised and sparsely employed.[69] Although their specificity is called into question,[153] inhibition assays remain attractive methods of study for their relevance, universal application, and wide comparability.[69]

5.2.2 Comparative analysis in other cell lines

Cells of different types are not uniformly affected by certain agents, be they nanomaterials or others.[167] Patra *et al.*[166] tested the effects of AuNPs on three cell lines, namely A549, BHK21 (baby hamster kidney) and HepG2 (human hepatocellular carcinoma). The AuNPs had varying effects on these three cell lines, even though treated identically; the A549 cells died, but the latter two cell types did not.[167] Another example of inter-cell-line differences is that with identical AuNPs, Vetten *et al.* found caveolae-mediated endocytosis to be the primary pathway for uptake in BEAS-2B cells in a monolayer culture.[50] It is further unclear whether the poor penetration observed in this study was due to NP factors or the characteristics (cell-packing, permeability and density) of the A549 cells. Therefore, comparative studies between various cell lines would be advantageous on multiple fronts. However, for the purposes of this study and the relevance hereof to environmental exposure and inhalation medicine, the A549 cell line was sufficient.

5.3 Recommendations for future work

5.3.1 In-depth characterisation and development of the A549 spheroid model

The first objective of this study was achieved successfully, with characterisation of morphological parameters and zones of viability and death. Thus, it is recommended that further characterisation of the same model is carried out in future – this will add insight to biological observations. In-depth genomic, proteomic, and metabolomic analyses, and applications or effects thereof[168-171] would be of value, further standardising protocols which may be followed universally. This would be instrumental in demystifying 3D *in vitro* techniques for the scientific community at large, given that spheroiding techniques are relatively poorly characterised.[172,173] This is in the best interests of the greater scientific community, as an inconsistent cell culture model produces unreliable results and creates large amounts of variation in any quantitative data generated, weakening conclusions based thereupon. Development of this platform would comprise inclusion of more dynamic culturing methods, allowing for prolonged culturing times and tighter control over growth and maturation of the spheroids.[22] Maturity of spheroids could be inferred from an understanding of when and how a dynamic equilibrium between nutrient depletion in growth media, as well as waste production therein.[4] A homeostatic steady state being reached by the spheroids in culture would increase their representation of the *in vivo* environment, strengthening conclusions drawn from this 3D *in vitro* model.[22,32]

5.3.2 Intercellular transport, penetration, and uptake kinetics studies

Findings in this study have identified pathways which were used by A549 spheroids to take up PCOOH-AuNPs, but were not able to prove subcellular and intercellular trafficking destinations, or fates of taken up PCOOH-AuNPs. Interactions with environmental proteins should also be characterised for these NPs such that accurate comparisons can be made in future. Such analyses can take place using liquid chromatography/mass spectrometry.

Intercellular transport and penetration into 3D structures should be investigated further via, among others, enhanced light microscopy, darkfield microscopy, CytoViva® 3D, and TEM[4,97,165] to further validate mechanisms used. Such investigations may assist in elucidating mechanisms of cytotoxicity, such as LMP resulting from lysosomal trafficking. Kinetic

evaluations may be valuable in benchmarking uptake processes for certain compounds. This would elucidate pathways employed secondarily over time, or in the event of a primary pathway no longer being available, as other pathways could be activated.[157]

5.3.3 Informing future nanoparticle design and testing thereof

The PCOOH-AuNPs in this study form part of a larger interest and have been specifically designed for a purpose. As previously mentioned, all NP-based studies make reference to the fact that NPs can be tailored to the needs of the user. Thus, from the findings in this study, NPs in future may be designed for enhanced penetration into spheroids, cytotoxicity, visualisation, uptake and particular uptake pathways. This may lead to additional avenues for manipulation of drugs and drug-delivery systems for better efficacy and lower cytotoxicity. Information obtained from the uptake and intracellular localisation studies can be used in the design of new drugs and chemical entities which would ultimately lead to more impactful implications in bioavailability and efficacy. A multidisciplinary approach would add value in such a case, with biological studies informing synthesis for tailored design.[42,81]

References

1. Medicines and Related Substances Act 101 of 1965 [online]. 1965 [cited 16 February, 2019]. Available from: https://www.hpcsa.co.za/Uploads/editor/UserFiles/downloads/legislations/acts/medicines_and_related_sub_act_101_of_1965.pdf.

2. International Conference on Harmonisation of Technical Requirements for Registration of Pharmaceuticals for Human Use [online]. 2008 [cited 16 February, 2019]. Available from: http://estri.ich.org/eCTD/eCTD_Specification_v3_2_2.pdf.

3. Hughes JP, Rees S, Kalindjian SB, Philpott KL. Principles of early drug discovery. Br J Pharmacol. 2011;162(6):1239-49.

4. Zanoni M, Piccinini F, Arienti C, Zamagni A, Santi S, Polico R, Bevilacqua A, Tesei A. 3D tumor spheroid models for *in vitro* therapeutic screening: a systematic approach to enhance the biological relevance of data obtained. Sci Rep. 2016;6:19103.

5. Roses AD. Pharmacogenetics in drug discovery and development: a translational perspective. Nat Rev Drug Disc. 2008;7(10):807-17.

6. Nadeau JH, Auwerx J. The virtuous cycle of human genetics and mouse models in drug discovery. Nat Rev Drug Disc. 2019;18(4):255-72.

7. Ekert JE, Johnson K, Strake B, Pardinas J, Jarantow S, Perkinson R, Colter DC. Three-dimensional lung tumor microenvironment modulates therapeutic compound responsiveness *in vitro*-implication for drug development. PLoS One. 2014;9(3):E92248.

8. DiMasi JA, Grabowski HG, Hansen RW. Innovation in the pharmaceutical industry: New estimates of R&D costs. J Health Econ. 2016;47:20-33.

9. Johnson JI, Decker S, Zaharevitz D, Rubinstein LV, Venditti JM, Schepartz S, Kalyandrug S, Christian M, Arbuck S, Hollingshead M, Sausville EA. Relationships between drug activity in NCI preclinical *in vitro* and *in vivo* models and early clinical trials. Br J Cancer. 2001;84:1424.

10. Moreno L, Pearson AD. How can attrition rates be reduced in cancer drug discovery? Expert Opin Drug Discov. 2013;8(4):363-8.

11. Kola I, Landis J. Can the pharmaceutical industry reduce attrition rates? Nat Rev Drug Discov. 2004;3(8):711-6.

12. Siramshetty VB, Nickel J, Omieczynski C, Gohlke B-O, Drwal MN, Preissner R. WITHDRAWN – a resource for withdrawn and discontinued drugs. Nucleic Acids Res. 2016;44(D1):1080-6.

13. Yamada KM, Cukierman E. Modeling tissue morphogenesis and cancer in 3D. Cell. 2007;130(4):601-10.

14. Alemany-Ribes M, Semino CE. Bioengineering 3D environments for cancer models. Adv Drug Deliv Rev. 2014;79-80:40-9.

15. Pampaloni F, Reynaud EG, Stelzer EH. The third dimension bridges the gap between cell culture and live tissue. Nat Rev Mol Cell Biol. 2007;8(10):839-45.

16. Kimlin LC, Casagrande G, Virador VM. *In vitro* three-dimensional (3D) models in cancer research: An update. Mol Carcinog. 2013;52(3):167-82.

17. Lee GY, Kenny PA, Lee EH, Bissell MJ. Three-dimensional culture models of normal and malignant breast epithelial cells. Nature Methods. 2007;4:359-65.

18. Ghajar CM, Bissell MJ. Tumor engineering: the other face of tissue engineering. Tissue Eng Part A. 2010;16(7):2153-6.

19. Maritan SM, Lian EY, Mulligan LM. An efficient and flexible cell aggregation method for 3D spheroid production. J Vis Exp. 2017(121):E55544.

20. Ravi M, Paramesh V, Kaviya SR, Anuradha E, Solomon FD. 3D cell culture systems: advantages and applications. J Cell Physiol. 2015;230(1):16-26.

21. Cui X, Hartanto Y, Zhang H. Advances in multicellular spheroids formation. J Royal Soc Interface. 2017;14(127).

22. Haycock JW. 3D cell culture: a review of current approaches and techniques. Methods Mol Biol. 2011;695:1-15.

23. Santini MT, Rainaldi G, Indovina PL. Apoptosis, cell adhesion and the extracellular matrix in the three-dimensional growth of multicellular tumor spheroids. Crit Rev Oncol Hematol. 2000;36(2-3):75-87.

24. Morrish F, Neretti N, Sedivy JM, Hockenbery DM. The oncogene c-Myc coordinates regulation of metabolic networks to enable rapid cell cycle entry. Cell Cycle. 2008;7(8):1054-66.

25. Theocharis AD, Skandalis SS, Gialeli C, Karamanos NK. Extracellular matrix structure. Adv Drug Deliv Rev. 2016;97:4-27.

26. da Rocha EL, Porto LM, Rambo CR. Nanotechnology meets 3D *in vitro* models: tissue engineered tumors and cancer therapies. Mater Sci Eng C Mater Biol Appl. 2014;34:270-9.

27. Bonnans C, Chou J, Werb Z. Remodelling the extracellular matrix in development and disease. Nat Rev Mol Cell Biol. 2014;15(12):786-801.

28. Nunes AS, Barros AS, Costa EC, Moreira AF, Correia IJ. 3D tumor spheroids as *in vitro* models to mimic *in vivo* human solid tumors resistance to therapeutic drugs. Biotechnol Bioeng. 2019;116(1):206-26.

29. Barrera-Rodríguez R, Fuentes JM. Multidrug resistance characterization in multicellular tumour spheroids from two human lung cancer cell lines. Cancer Cell Int. 2015;15:47-8.

30. Wartenberg M, Ling FC, Muschen M, Klein F, Acker H, Gassmann M, Petrat K, Putz V, Hescheler J, Sauer H. Regulation of the multidrug resistance transporter P-glycoprotein in multicellular tumor spheroids by hypoxia-inducible factor (HIF-1) and reactive oxygen species. FASEB J. 2003;17(3):503-5.

31. Achilli T-M, Meyer J, Morgan JR. Advances in the formation, use and understanding of multi-cellular spheroids. Expert Opin Biol Ther. 2012;12(10):1347-60.

32. Sambale F, Lavrentieva A, Stahl F, Blume C, Stiesch M, Kasper C, Bahnemann D, Scheper T. Three dimensional spheroid cell culture for nanoparticle safety testing. J Biotechnol. 2015;205:120-9.

33. Costa EC, de Melo-Diogo D, Moreira AF, Carvalho MP, Correia IJ. Spheroids formation on non-adhesive surfaces by liquid overlay technique: considerations and practical approaches. Biotechnol J. 2018;13(1).

34. Lee J, Cuddihy MJ, Kotov NA. Three-dimensional cell culture matrices: state of the art. Tissue engineering Part B, Reviews. 2008;14(1):61-86.

35. Kou L, Sun J, Zhai Y, He Z. The endocytosis and intracellular fate of nanomedicines: implication for rational design. Asian J Pharm. 2013;8(1):1-10.

36. Lazzari G, Couvreur P, Mura S. Multicellular tumor spheroids: a relevant 3D model for the *in vitro* preclinical investigation of polymer nanomedicines. Polym Chem. 2017;8(34):4947-69.

37. Sutradhar KB, Amin ML. Nanotechnology in cancer drug delivery and selective targeting. ISRN Nanotech. 2014;1:12-3.

38. Mayer EL, Burstein HJ. Chemotherapy for metastatic breast cancer. Hematol Oncol Clin North Am. 2007;21(2):257-72.

39. Bahrami B, Hojjat-Farsangi M, Mohammadi H, Anvari E, Ghalamfarsa G, Yousefi M, Jadidi-Niaragh F. Nanoparticles and targeted drug delivery in cancer therapy. Immunol Lett. 2017;190:64-83.

40. Sztandera K, Gorzkiewicz M, Klajnert-Maculewicz B. Gold nanoparticles in cancer treatment. Mol Pharm. 2019;16(1):1-23.

41. Faraji AH, Wipf P. Nanoparticles in cellular drug delivery. Bioorg Med Chem. 2009;17(8):2950-62.

42. Safari J, Zarnegar Z. Advanced drug delivery systems: nanotechnology of health design: a review. J Saudi Chem Soc. 2014;18(2):85-99.

43. Chithrani BD, Ghazani AA, Chan WCW. Determining the size and shape dependence of gold nanoparticle uptake into mammalian cells. Nano Lett. 2006;6(4):662-8.

44. Lim Z-ZJ, Li J-EJ, Ng C-T, Yung L-YL, Bay B-H. Gold nanoparticles in cancer therapy. Acta Pharmacol Sin. 2011;32(8):983-90.

45. Dykman L, Khlebtsov N. Gold nanoparticles in biomedical applications: recent advances and perspectives. Chem Soc Rev. 2012;41(6):2256-82.

46. Ahn S, Lee I-H, Kang S, Kim D, Choi M, Saw PE, Shin E-C, Jon S. Gold nanoparticles displaying tumor-associated self-antigens as a potential vaccine for cancer immunotherapy. Adv Healthc Mater. 2014;3(8):1194-9.

47. Hainfeld JF, Dilmanian FA, Slatkin DN, Smilowitz HM. Radiotherapy enhancement with gold nanoparticles. J Pharm Pharmacol. 2008;60(8):977-85.

48. Arvizo RR, Rana S, Miranda OR, Bhattacharya R, Rotello VM, Mukherjee P. Mechanism of anti-angiogenic property of gold nanoparticles: role of nanoparticle size and surface charge. Nanomedicine. 2011;7(5):580-7.

49. Marchesan S, Prato M. Nanomaterials for (nano)medicine. ACS Med Chem Lett. 2013;4(2):147-9.

50. Vetten M, Gulumian M. Differences in uptake of 14 nm PEG-liganded gold nanoparticles into BEAS-2B cells is dependent on their functional groups. Toxicol Appl Pharmacol. 2019;363:131-41.

51. Dreaden EC, Austin LA, Mackey MA, El-Sayed MA. Size matters: gold nanoparticles in targeted cancer drug delivery. Ther Deliv. 2012;3(4):457-78.

52. Zhou X, Xu W, Liu G, Panda D, Chen P. Size-dependent catalytic activity and dynamics of gold nanoparticles at the single-molecule level. J Am Chem Soc. 2009;132(1):138-46.

53. Libutti SK, Paciotti GF, Byrnes AA, Alexander HR, Jr., Gannon WE, Walker M, Seidel GD, Yuldasheva N, Tamarkin L. Phase I and pharmacokinetic studies of CYT-6091, a novel PEGylated colloidal gold-rhTNF nanomedicine. Clin Cancer Res. 2010;16(24):6139-49.

54. Bobo D, Robinson KJ, Islam J, Thurecht KJ, Corrie SR. Nanoparticle-based medicines: A review of FDA-approved materials and clinical trials to date. Pharm Res. 2016;33(10):2373-87.

55. Gulumian M, Andraos C. In search of a converging cellular mechanism in nanotoxicology and nanomedicine in the treatment of cancer. Toxicol Pathol. 2018;46(1):4-13.

56. Lamela H, Jara F, Cunningham V. Modelling and characterization of photothermal effects assisted with gold nanorods in ex-vivo samples and in a murine model. Proc of SPIE. 2011;7901.

57. Jenkins SV, Nedosekin DA, Shaulis BJ, Wang T, Jamshidi-Parsian A, Pollock ED, Chen J, Dings RPM, Griffin RJ. Enhanced photothermal treatment efficacy and normal tissue protection via vascular targeted gold nanocages. Nanotheranostics. 2019;3(2):145-55.

58. Efficacy study of AuroLase therapy in subjects with primary and/or metastatic lung tumors [online]. Nanospectra Biosciences, Inc.; 2016 [cited 10 November, 2020]. Available from: https://clinicaltrials.gov/ct2/show/NCT01679470.

59. Bhattacharyya K, Mehta S, Viator J. Optically absorbing nanoparticle mediated cell membrane permeabilization. Opt Lett. 2012;37(21):4474-6.

60. Oh N, Park J-H. Endocytosis and exocytosis of nanoparticles in mammalian cells. Int J Nanomed. 2014;9(Suppl 1):51-63.

61. Conner SD, Schmid SL. Regulated portals of entry into the cell. Nature. 2003;422(6927):37-44.

62. Iversen T-G, Skotland T, Sandvig K. Endocytosis and intracellular transport of nanoparticles: Present knowledge and need for future studies. Nano Today. 2011;6(2):176-85.

63. Gary-Bobo M, Vaillant O, Maynadier M, Basile I, Gallud A, El Cheikh K, Bouffard E, Morère A, Rébillard X, Puche P, Nirdé P, Garcia M. Targeting multiplicity: the key factor for anti-cancer nanoparticles. Curr Med Chem. 2013;20(15):1946-55.

64. Ding H-M, Ma Y-Q. Role of physicochemical properties of coating ligands in receptor-mediated endocytosis of nanoparticles. Biomaterials. 2012;33(23):5798-802.

65. Le Bihan O, Bonnafous P, Marak L, Bickel T, Trepout S, Mornet S, De Haas F, Talbot H, Taveau JC, Lambert O. Cryo-electron tomography of nanoparticle transmigration into liposome. J Struct Biol. 2009;168(3):419-25.

66. Vácha R, Martinez-Veracoechea FJ, Frenkel D. Receptor-mediated endocytosis of nanoparticles of various shapes. Nano Lett. 2011;11(12):5391-5.

67. Rothen-Rutishauser BM, Schürch S, Haenni B, Kapp N, Gehr P. Interaction of fine particles and nanoparticles with red blood cells visualized with advanced microscopic techniques. Environ Sci Technol. 2006;40(14):4353-9.

68. Verma A, Stellacci F. Effect of surface properties on nanoparticle-cell interactions. Small. 2010;6(1):12-21.

69. Manzanares D, Ceña V. Endocytosis: the nanoparticle and submicron nanocompounds gateway into the cell. Pharmaceutics. 2020;12(4):371-93.

70. Piao S, Amaravadi RK. Targeting the lysosome in cancer. Ann N Y Acad Sci. 2016;1371(1):45-54.

71. Behzadi S, Serpooshan V, Tao W, Hamaly MA, Alkawareek MY, Dreaden EC, Brown D, Alkilany AM, Farokhzad OC, Mahmoudi M. Cellular uptake of nanoparticles: journey inside the cell. Chem Soc Rev. 2017;46(14):4218-44.

72. Lim JP, Gleeson PA. Macropinocytosis: an endocytic pathway for internalising large gulps. Immunol Cell Biol. 2011;89(8):836-43.

73. Mayor S, Pagano RE. Pathways of clathrin-independent endocytosis. Nat Rev Mol Cell Biol. 2007;8(8):603-12.

74. Bewersdorff T, Vonnemann J, Kanik A, Haag R, Haase A. The influence of surface charge on serum protein interaction and cellular uptake: studies with dendritic polyglycerols and dendritic polyglycerol-coated gold nanoparticles. Int J Nanomed. 2017;12:2001-19.

75. Tang Z, Scherer PE, Okamoto T, Song K, Chu C, Kohtz DS, Nishimoto I, Lodish HF, Lisanti MP. Molecular cloning of caveolin-3, a novel member of the caveolin gene family expressed predominantly in muscle. J Biol Chem. 1996;271(4):2255-61.

76. Kasamatsu H, Nakanishi A. How do animal DNA viruses get to the nucleus? Annu Rev Microbiol. 1998;52:627-86.

77. Hillaireau H, Couvreur P. Nanocarriers' entry into the cell: relevance to drug delivery. Cell Mol Life Sci. 2009;66(17):2873-96.

78. Benmerah A, Lamaze C. Clathrin-coated pits: vive la difference? Traffic. 2007;8(8):970-82.

79. Lamaze C, Dujeancourt A, Baba T, Lo CG, Benmerah A, Dautry-Varsat A. Interleukin 2 receptors and detergent-resistant membrane domains define a clathrin-independent endocytic pathway. Mol Cell. 2001;7(3):661-71.

80. Damke H, Baba T, van der Bliek AM, Schmid SL. Clathrin-independent pinocytosis is induced in cells overexpressing a temperature-sensitive mutant of dynamin. J Cell Biol. 1995;131(1):69-80.

81. Savolainen K, Alenius H, Norppa H, Pylkkänen L, Tuomi T, Kasper G. Risk assessment of engineered nanomaterials and nanotechnologies — a review. Toxicology. 2010;269(2):92-104.

82. Vetten MA, Tlotleng N, Tanner Rascher D, Skepu A, Keter FK, Boodhia K, Koekemoer LA, Andraos C, Tshikhudo R, Gulumian M. Label-free *in vitro* toxicity and uptake assessment of citrate stabilised gold nanoparticles in three cell lines. Part Fibre Toxicol. 2013;10:50-65.

83. Thurn KT, Brown E, Wu A, Vogt S, Lai B, Maser J, Paunesku T, Woloschak GE. Nanoparticles for applications in cellular imaging. Nanoscale Res Lett. 2007;2(9):430-41.

84. Malugin A, Ghandehari H. Cellular uptake and toxicity of gold nanoparticles in prostate cancer cells: a comparative study of rods and spheres. J Appl Toxicol. 2010;30(3):212-7.

85. Jiang W, Kim BYS, Rutka JT, Chan WCW. Nanoparticle-mediated cellular response is size-dependent. Nat Nanotechnol. 2008;3(3):145-50.

86. Zhang S, Li J, Lykotrafitis G, Bao G, Suresh S. Size-dependent endocytosis of nanoparticles. Adv Mater. 2009;21:419-24.

87. Shang L, Nienhaus K, Nienhaus GU. Engineered nanoparticles interacting with cells: size matters. J Nanobiotechnology. 2014;12(1):5-16.

88. England CG, Gobin AM, Frieboes HB. Evaluation of uptake and distribution of gold nanoparticles in solid tumors. Eur Phys J Plus. 2015;130(11):231-58.

89. Sperling RA, Parak WJ. Surface modification, functionalization and bioconjugation of colloidal inorganic nanoparticles. Philos Trans A Math Phys Eng Sci. 2010;368(1915):1333-83.

90. Vercauteren D, Vandenbroucke RE, Jones AT, Rejman J, Demeester J, De Smedt SC, Sanders NN, Braeckmans K. The use of inhibitors to study endocytic pathways of gene carriers: optimization and pitfalls. Mol Ther. 2010;18(3):561-9.

91. Wolfbeis OS. An overview of nanoparticles commonly used in fluorescent bioimaging. Chem Soc Rev. 2015;44(14):4743-68.

92. Ivanov AI. Pharmacological inhibition of endocytic pathways: is it specific enough to be useful? In: Ivanov AI, editor. Exocytosis and Endocytosis. Totowa, NJ: Humana Press; 2008. p. 15-33.

93. Han S-C, Guo H-C, Sun S-Q, Jin Y, Wei Y-Q, Feng X, Yao X-P, Cao S-Z, Xiang Liu D, Liu X-T. Productive entry of foot-and-mouth disease virus via macropinocytosis independent of phosphatidylinositol 3-kinase. Sci Rep. 2016;6(1).

94. CytoViva® Hyperspectral User Manual Auburn, AL, USA CytoViva, Inc. [online]. 2011 [cited 21 February, 2020]. Available from: https://cytoviva.com/wp-content/documents/hyperspectral/products/HSI-User-Manual-8-11-11.pdf.

95. Boyoglu C, He Q, Willing G, Boyoglu-Barnum S, Dennis VA, Pillai S, Singh SR. Microscopic studies of various sizes of gold nanoparticles and their cellular localizations. ISRN Nanotech. 2013;2013:123838.

96. Sabella S, Carney RP, Brunetti V, Malvindi MA, Al-Juffali N, Vecchio G, Janes SM, Bakr OM, Cingolani R, Stellacci F. A general mechanism for intracellular toxicity of metal-containing nanoparticles. Nanoscale. 2014;6(12):7052-61.

97. Uboldi C, Bonacchi D, Lorenzi G, Hermanns MI, Pohl C, Baldi G, Unger RE, Kirkpatrick CJ. Gold nanoparticles induce cytotoxicity in the alveolar type-II cell lines A549 and NCIH441. Part Fibre Toxicol. 2009;6:18-30.

98. Alkilany AM, Murphy CJ. Toxicity and cellular uptake of gold nanoparticles: what we have learned so far? J Nanopart Res. 2010;12(7):2313-33.

99. Pan Y, Neuss S, Leifert A, Fischler M, Wen F, Simon U, Schmid G, Brandau W, Jahnen-Dechent W. Size-dependent cytotoxicity of gold nanoparticles. Small. 2007;3(11):1941-9.

100. Niidome T, Yamagata M, Okamoto Y, Akiyama Y, Takahashi H, Kawano T, Katayama Y, Niidome Y. PEG-modified gold nanorods with a stealth character for *in vivo* applications. J Control Release. 2006;114(3):343-7.

101. Tlotleng N, Vetten MA, Keter FK, Skepu A, Tshikhudo R, Gulumian M. Cytotoxicity, intracellular localization and exocytosis of citrate capped and PEG functionalized gold nanoparticles in human hepatocyte and kidney cells. Cell Biol Toxicol. 2016;32(4):305-21.

102. Khlebtsov N, Dykman L. Biodistribution and toxicity of engineered gold nanoparticles: a review of *in vitro* and *in vivo* studies. Chem Soc Rev. 2011;40(3):1647-71.

103. Nath S, Devi GR. Three-dimensional culture systems in cancer research: Focus on tumor spheroid model. Pharmacol Ther. 2016;163:94-108.

104. Baek N, Seo OW, Kim M, Hulme J, An SSA. Monitoring the effects of doxorubicin on 3D-spheroid tumor cells in real-time. Onco Targets Ther. 2016;9:7207-18.

105. Friedrich J, Eder W, Castaneda J, Doss M, Huber E, Ebner R, Kunz-Schughart LA. A reliable tool to determine cell viability in complex 3-d culture: the acid phosphatase assay. J Biomol Screen. 2007;12(7):925-37.

106. Senavirathna LK, Fernando R, Maples D, Zheng Y, Polf JC, Ranjan A. Tumor Spheroids as an *in vitro* model for determining the therapeutic response to proton beam radiotherapy and thermally sensitive nanocarriers. Theranostics. 2013;3(9):687-91.

107. Riss T, Moravec R. Introducing the CytoTox-ONE homogeneous membrane integrity assay. Cell Notes. 2002;4:6-9.

108. Jones KH, Senft JA. An improved method to determine cell viability by simultaneous staining with fluorescein diacetate-propidium iodide. J Histochem Cytochem. 1985;33(1):77-9.

109. Vichai V, Kirtikara K. Sulforhodamine B colorimetric assay for cytotoxicity screening. Nat Protoc. 2006;1(3):1112-6.

110. Promega CytoTox-ONE™ homogeneous membrane integrity assay technical bulletin [online]. Madison, WI, USA Promega Corporation; 2009 [cited 20 April, 2020]. Available from: https://worldwide.promega.com/Resources/Protocols/Technical%20Bulletins/101/CytoTox%20ONE%20Homogeneous%20Membrane%20Integrity%20Assay%20Protocol/.

111. Ong KJ, MacCormack TJ, Clark RJ, Ede JD, Ortega VA, Felix LC, Dang MKM, Ma G, Fenniri H, Veinot JGC, Goss GG. Widespread nanoparticle-assay interference: implications for nanotoxicity testing. PLoS One. 2014;9(3):E90650.

112. Andraos C, Yu IJ, Gulumian M. Interference: a much-neglected aspect in high-throughput screening of nanoparticles. Int J Toxicol. 2020;39(5):397-421.

113. Kroll A, Pillukat MH, Hahn D, Schnekenburger J. Interference of engineered nanoparticles with *in vitro* toxicity assays. Arch Toxicol. 2012;86(7):1123-36.

114. ATCC product sheet: A549 (ATCC® CCL-185™) Manassas, VA, USA: American Type Culture Collection [online]. 2019 [cited 20 April, 2020]. Available from: https://www.atcc.org/products/all/CCL-185.aspx#documentation.

115. Meenach SA, Tsoras AN, McGarry RC, Mansour HM, Hilt JZ, Anderson KW. Development of three-dimensional lung multicellular spheroids in air- and liquid-interface culture for the evaluation of anticancer therapeutics. Int J Oncol. 2016;48(4):1701-9.

116. Mohapatra S, Nandi S, Chowdhury R, Das G, Ghosh S, Bhattacharyya K. Spectral mapping of 3D multi-cellular tumor spheroids: time-resolved confocal microscopy. Phys Chem Chem Phys. 2016;18(27):18381-90.

117. Gulumian M, Verbeek J, Andraos C, Sanabria N, de Jager P. Systematic review of screening and surveillance programs to protect workers from nanomaterials. PLoS One. 2016;11(11):e0166071.

118. Mansour HM, Rhee Y-S, Wu X. Nanomedicine in pulmonary delivery. Int J Nanomed. 2009;4:299-319.

119. Zhang XD, Wu HY, Wu D, Wang YY, Chang JH, Zhai ZB, Meng AM, Liu PX, Zhang LA, Fan FY. Toxicologic effects of gold nanoparticles *in vivo* by different administration routes. Int J Nanomed. 2010;5:771-81.

120. De Jong WH, Borm PJA. Drug delivery and nanoparticles:applications and hazards. Int J Nanomed. 2008;3(2):133-49.

121. Zernike F. How I discovered phase contrast. Science. 1955;121(3141):345-9.

122. Ivanov DP, Parker TL, Walker DA, Alexander C, Ashford MB, Gellert PR, Garnett MC. Multiplexing spheroid volume, resazurin and acid phosphatase viability assays for high-throughput screening of tumour spheroids and stem cell neurospheres. PLoS One. 2014;9(8):e103817.

123. Chen W, Wong C, Vosburgh E, Levine AJ, Foran DJ, Xu EY. High-throughput image analysis of tumor spheroids: a user-friendly software application to measure the size of spheroids automatically and accurately. J Vis Exp. 2014(89):E51639.

124. Kramer DN, Guilbault GG. A substrate for the fluorometric determination of lipase activity. Anal Chem. 1963;35(4):588-9.

125. Boyd V, Cholewa OM, Papas KK. Limitations in the use of fluorescein diacetate/propidium iodide (FDA/PI) and cell permeable nucleic acid stains for viability measurements of isolated islets of Langerhans. Curr Trends Biotechnol Pharm. 2008;2(2):66-84.

126. Zhu H, Zhou B, Chan L, Du Y, Chen T. Transferrin-functionalized nanographene oxide for delivery of platinum complexes to enhance cancer-cell selectivity and apoptosis-inducing efficacy. Int J Nanomed. 2017;12:5023-38.

127. Macia E, Ehrlich M, Massol R, Boucrot E, Brunner C, Kirchhausen T. Dynasore, a cell-permeable inhibitor of dynamin. Dev Cell. 2006;10:839-50.

128. Commisso C, Flinn RJ, Bar-Sagi D. Determining the macropinocytic index of cells through a quantitative image-based assay. Nat Protoc. 2014;9(1):182-92.

129. Roth GA, Sosa Peña Mdel P, Neu-Baker NM, Tahiliani S, Brenner SA. Identification of metal oxide nanoparticles in histological samples by enhanced darkfield microscopy and hyperspectral mapping. J Vis Exp. 2015(106):e53317.

130. Sethi P, Jyoti A, Swindell EP, Chan R, Langner UW, Feddock JM, Nagarajan R, O'Halloran TV, Upreti M. 3D tumor tissue analogs and their orthotopic implants for understanding tumor-targeting of microenvironment-responsive nanosized chemotherapy and radiation. Nanomedicine. 2015;11(8):2013-23.

131. Vinci M, Gowan S, Boxall F, Patterson L, Zimmermann M, Court W, Lomas C, Mendiola M, Hardisson D, Eccles SA. Advances in establishment and analysis of three-dimensional tumor spheroid-based functional assays for target validation and drug evaluation. BMC Biol. 2012;10(1):29-50.

132. De Sousa EMF, Vermeulen L, Fessler E, Medema JP. Cancer heterogeneity – a multifaceted view. EMBO reports. 2013;14(8):686-95.

133. Goodman CM, McCusker CD, Yilmaz T, Rotello VM. Toxicity of gold nanoparticles functionalized with cationic and anionic side chains. Bioconjug Chem. 2004;15(4):897-900.

134. Subara D, Jaswir I. Gold nanoparticles: synthesis and application for Halal authentication in meat and meat Products. Int J Adv Sci Eng Inf Technol. 2018;8 (2018):1633-41.

135. Shi J, Kantoff PW, Wooster R, Farokhzad OC. Cancer nanomedicine: progress, challenges and opportunities. Nat Rev Cancer. 2017;17(1):20-37.

136. Ding L, Yao C, Yin X, Li C, Huang Y, Wu M, Wang B, Guo X, Wang Y, Wu M. Size, shape, and protein corona determine cellular uptake and removal mechanisms of gold nanoparticles. Small. 2018;14(42):E1801451.

137. Kiss AL. Caveolae and the regulation of endocytosis. Adv Exp Med Biol. 2012;729:14-28.

138. Connor EE, Mwamuka J, Gole A, Murphy CJ, Wyatt MD. Gold nanoparticles are taken up by human cells but do not cause acute cytotoxicity. Small. 2005;1(3):325-7.

139. Zhao Z, Ukidve A, Krishnan V, Mitragotri S. Effect of physicochemical and surface properties on *in vivo* fate of drug nanocarriers. Adv Drug Deliv Rev. 2019;143:3-21.

140. Semple SC, Chonn A, Cullis PR. Interactions of liposomes and lipid-based carrier systems with blood proteins: relation to clearance behaviour *in vivo*. Adv Drug Deliv Rev. 1998;32(1):3-17.

141. Kumari S, Mg S, Mayor S. Endocytosis unplugged: multiple ways to enter the cell. Cell Res. 2010;20(3):256-75.

142. Lu Y, Low PS. Folate-mediated delivery of macromolecular anticancer therapeutic agents. Adv Drug Deliv Rev. 2002;54(5):675-93.

143. Kelemen LE. The role of folate receptor alpha in cancer development, progression and treatment: cause, consequence or innocent bystander? Int J Cancer. 2006;119(2):243-50.

144. Wang F, Bexiga MG, Anguissola S, Boya P, Simpson JC, Salvati A, Dawson KA. Time resolved study of cell death mechanisms induced by amine-modified polystyrene nanoparticles. Nanoscale. 2013;5(22):10868-76.

145. Sipos A, Kim KJ, Sioutas C, Crandall ED. Evidence for nanoparticle-induced lysosomal dysfunction in lung adenocarcinoma (A549) cells. Int J Mol Sci. 2019;20(21):5253-69.

146. Wang F, Gómez-Sintes R, Boya P. Lysosomal membrane permeabilization and cell death. Traffic. 2018;19(12):918-31.

147. Niora M, Pedersbæk D, Münter R, Weywadt MFdV, Farhangibarooji Y, Andresen TL, Simonsen JB, Jauffred L. Head-to-head comparison of the penetration efficiency of lipid-based nanoparticles into tumor spheroids. ACS Omega. 2020;5(33):21162-71.

148. Harush-Frenkel O, Debotton N, Benita S, Altschuler Y. Targeting of nanoparticles to the clathrin-mediated endocytic pathway. Biochem Biophys Res Commun. 2007;353(1):26-32.

149. Elci SG, Jiang Y, Yan B, Kim ST, Saha K, Moyano DF, Yesilbag Tonga G, Jackson LC, Rotello VM, Vachet RW. Surface charge controls the suborgan biodistributions of gold nanoparticles. ACS Nano. 2016;10(5):5536-42.

150. Balfourier A, Luciani N, Wang G, Lelong G, Ersen O, Khelfa A, Alloyeau D, Gazeau F, Carn F. Unexpected intracellular biodegradation and recrystallization of gold nanoparticles. Proc Natl Acad Sci U S A. 2020;117(1):103-13.

151. Pelkmans L, Helenius A. Endocytosis via caveolae. Traffic. 2002;3(5):311-20.

152. Gradishar WJ. Albumin-bound paclitaxel: a next-generation taxane. Expert Opin Pharmacother. 2006;7(8):1041-53.

153. Rejman J, Bragonzi A, Conese M. Role of clathrin- and caveolae-mediated endocytosis in gene transfer mediated by lipo- and polyplexes. Mol Ther. 2005;12(3):468-74.

154. Epstein T, Gatenby RA, Brown JS. The Warburg effect as an adaptation of cancer cells to rapid fluctuations in energy demand. PLoS One. 2017;12(9):e0185085.

155. Di Nicolantonio F, Mercer SJ, Knight LA, Gabriel FG, Whitehouse PA, Sharma S, Fernando A, Glaysher S, Di Palma S, Johnson P, Somers SS, Toh S, Higgins B, Lamont A, Gulliford T, Hurren J, Yiangou C, Cree IA. Cancer cell adaptation to chemotherapy. BMC Cancer. 2005;5:78-84.

156. Di Fiore PP, von Zastrow M. Endocytosis, signaling, and beyond. Cold Spring Harb Perspect Biol. 2014;6(8):a016865.

157. dos Santos T, Varela J, Lynch I, Salvati A, Dawson KA. Effects of transport inhibitors on the cellular uptake of carboxylated polystyrene nanoparticles in different cell lines. PLoS One. 2011;6(9):e24438-e.

158. Medina-Kauwe LK. "Alternative" endocytic mechanisms exploited by pathogens: new avenues for therapeutic delivery? Adv Drug Deliv Rev. 2007;59(8):798-809.

159. Anderson HA, Chen Y, Norkin LC. Bound simian virus 40 translocates to caveolin-enriched membrane domains, and its entry is inhibited by drugs that selectively disrupt caveolae. Mol Biol Cell. 1996;7(11):1825-34.

160. Pelkmans L, Kartenbeck J, Helenius A. Caveolar endocytosis of simian virus 40 reveals a new two-step vesicular-transport pathway to the ER. Nat Cell Biol. 2001;3(5):473-83.

161. Aguzzi A. Prions and the immune system: a journey through gut, spleen, and nerves. Adv Immunol. 2003;81:123-71.

162. Haïk S, Faucheux BA, Hauw JJ. Brain targeting through the autonomous nervous system: lessons from prion diseases. Trends Mol Med. 2004;10(3):107-12.

163. Lord JM, Roberts LM. Toxin entry: retrograde transport through the secretory pathway. J Cell Biol. 1998;140(4):733-6.

164. Perrault SD, Walkey C, Jennings T, Fischer HC, Chan WCW. Mediating Tumor Targeting Efficiency of Nanoparticles Through Design. Nano Lett. 2009;9(5):1909-15.

165. Cabral H, Matsumoto Y, Mizuno K, Chen Q, Murakami M, Kimura M, Terada Y, Kano MR, Miyazono K, Uesaka M, Nishiyama N, Kataoka K. Accumulation of sub-100 nm

polymeric micelles in poorly permeable tumours depends on size. Nat Nanotechnol. 2011;6(12):815-23.

166. Preta G, Cronin J, Sheldon I. Dynasore — not just a dynamin inhibitor. Cell Commun Signal. 2015;13.

167. Patra HK, Banerjee S, Chaudhuri U, Lahiri P, Dasgupta AK. Cell selective response to gold nanoparticles. Nanomedicine. 2007;3(2):111-9.

168. Herland A, Maoz BM, FitzGerald EA, Grevesse T, Vidoudez C, Sheehy SP, Budnik N, Dauth S, Mannix R, Budnik B, Parker KK, Ingber DE. Proteomic and metabolomic characterization of human neurovascular unit cells in response to methamphetamine. Adv Biosys. 2020:E1900230.

169. McMahon KM, Volpato M, Chi HY, Musiwaro P, Poterlowicz K, Peng Y, Scally AJ, Patterson LH, Phillips RM, Sutton CW. Characterization of changes in the proteome in different regions of 3D multicell tumor spheroids. J Proteome Res. 2012;11(5):2863-75.

170. Margalit A, Kavanagh K, Carolan JC. Characterization of the proteomic response of A549 cells following sequential exposure to Aspergillus fumigatus and Pseudomonas aeruginosa. J Proteome Res. 2020;19(1):279-91.

171. Huang Y, Lu Y, Vadlamudi M, Zhao S, Felmlee M, Rahimian R, Guo X. Intrapulmonary inoculation of multicellular spheroids to construct an orthotopic lung cancer xenograft model that mimics four clinical stages of non-small cell lung cancer. J Pharmacol Toxicol Methods. 2020;104:E106885.

172. Mehta G, Hsiao AY, Ingram M, Luker GD, Takayama S. Opportunities and challenges for use of tumor spheroids as models to test drug delivery and efficacy. J Control Release. 2012;164(2):192-204.

173. Lee JM, Park DY, Yang L, Kim E-J, Ahrberg CD, Lee K-B, Chung BG. Generation of uniform-sized multicellular tumor spheroids using hydrogel microwells for advanced drug screening. Sci Rep. 2018;8(1):E17145.

UNIVERSITEIT VAN PRETORIA
UNIVERSITY OF PRETORIA
YUNIBESITHI YA PRETORIA

Appendix I: Ethical approval

UNIVERSITEIT VAN PRETORIA
UNIVERSITY OF PRETORIA
YUNIBESITHI YA PRETORIA

Faculty of Health Sciences

Institution: The Research Ethics Committee, Faculty Health Sciences, University of Pretoria complies with ICH-GCP guidelines and has US Federal wide Assurance.

- FWA 00002567, Approved dd 22 May 2002 and Expires 03/20/2022.
- IORG #: IORG0001762 OMB No. 0990-0279 Approved for use through February 28, 2022 and Expires: 03/04/2023.

20 July 2020

Approval Certificate
Annual Renewal

Ethics Reference No.: 540/2019
Title: Mechanisms facilitating uptake of carboxyl-polyethylene glycol-functionalised gold nanoparticles into multicellular spheroids

Dear Mr S Fobian

The **Annual Renewal** as supported by documents received between 2020-06-29 and 2020-07-15 for your research, was approved by the Faculty of Health Sciences Research Ethics Committee on its quorate meeting of 2020-07-15.

Please note the following about your ethics approval:

- Renewal of ethics approval is valid for 1 year, subsequent annual renewal will become due on 2021-07-20.
- Please remember to use your protocol number (540/2019) on any documents or correspondence with the Research Ethics Committee regarding your research.
- Please note that the Research Ethics Committee may ask further questions, seek additional information, require further modification, monitor the conduct of your research, or suspend or withdraw ethics approval.

Ethics approval is subject to the following:

- The ethics approval is conditional on the research being conducted as stipulated by the details of all documents submitted to the Committee. In the event that a further need arises to change who the investigators are, the methods or any other aspect, such changes must be submitted as an Amendment for approval by the Committee.

We wish you the best with your research.

Yours sincerely

Dr R Sommers
MBChB MMed (Int) MPharmMed PhD
Deputy Chairperson of the Faculty of Health Sciences Research Ethics Committee, University of Pretoria

The Faculty of Health Sciences Research Ethics Committee complies with the SA National Act 61 of 2003 as it pertains to health research and the United States Code of Federal Regulations Title 45 and 46. This committee abides by the ethical norms and principles for research, established by the Declaration of Helsinki, the South African Medical Research Council Guidelines as well as the Guidelines for Ethical Research: Principles Structures and Processes, Second Edition 2015 (Department of Health)

Research Ethics Committee
Room 4-60, Level 4, Tswelopele Building
University of Pretoria, Private Bag x323
Gezina 0031, South Africa
Tel +27 (0)12 356 3084
Email: deepeka.behari@up.ac.za
www.up.ac.za

Fakulteit Gesondheidswetenskappe
Lefapha la Disaense tša Maphelo

Appendix II: Reagents List

5-(N-ethyl-N-isopropyl) amiloride

5-(N-ethyl-N-isopropyl) amiloride (EIPA) was procured from Merck (Darmstadt, Germany) as a dry powder and stored at 4°C. A 300 mM solution was created by dissolving 9.75 mg of dry powder in 500 µL DMSO. An aliquot of 500 µL was stored at -80°C.

A549 cells

A549 alveolar carcinoma cells were procured from the ATCC (Manassas, USA) (ATCC® CCL-185™) as a frozen vial of cell suspension. Cells were thawed, then cultured and passaged within the Department of Pharmacology, University of Pretoria.

Agarose

Low-gelling temperature agarose was procured from Merck (Darmstadt, Germany), and stored as a powder at room temperature. A 4% (w/v) solution was created by dissolving 1 g of agarose powder in 100 mL of DMEM. The solution was autoclaved for sterility and to facilitate dissolution, then kept at 4°C until needed. Prior to use, the mixture was heated in a microwave to allow for liquidisation, then diluted in FCS-free DMEM to 1.6% (w/v).

Chlorpromazine

Chlorpromazine was procured from Merck (Darmstadt, Germany) as a dry powder and stored at 20°C. A 1 mM solution was created by dissolving 1.59 mg of dry powder in 5 mL dH2O. Aliquots of 100 µL were stored at -80°C.

Dimethyl sulfoxide

Dimethyl sulfoxide (DMSO) was procured as a liquid from Merck (Darmstadt, Germany). As a vehicle, pure DMSO was used. To obtain a 0.4% vehicle control, 20 µL pure DMSO was dissolved in 4.98 mL DMEM directly prior to experimentation.

Distilled water

Distilled water (dH2O) was distilled using an ELGA PURELAB® Chorus water purification system, and autoclaved when necessary for sterility.

Dynasore

Dynasore was procured from Merck (Darmstadt, Germany) as a dry powder and stored in the dark at -20°C. To make a 100 mM solution, 3.2 mg of dry powder was dissolved in 100 µL DMSO. Aliquots of 50 µL were stored at -80°C.

Ethanol

Ethanol (EtOH) was procured from Merck (Darmstadt, Germany), and stored as a liquid at room temperature until use in maintaining sterility during experimentation. A dilution to 70% was made in dH2O when needed for sterilisation of the workplace including countertops, the

laminar flow cabinet surfaces and any vessels being introduced to the sterile environment.

Foetal calf serum Foetal calf serum, procured from Merck (Darmstadt, Germany), was heat-inactivated by incubating at 56°C for 40 min. The solution was stored at -20°C in the dark until needed. Dilutions were made in medium as described in Section 2.5.

Genistein Genistein was procured from Merck (Darmstadt, Germany) as a dry powder and stored at 0°C. A 100 mM solution was created by dissolving 1.35 mg of dry powder in 50 µL DMSO. Aliquots of 50 µL were stored at -80°C.

Live/dead staining solution The fluorescent dyes, propidium iodide (PI) and fluorescein diacetate (FDA) were procured from Merck (Darmstadt, Germany), and stored as powders at 4°C until needed. A single staining solution (of concentrations 4 µg/mL [PI] and 5 µg/mL [FDA]) was prepared by dissolving 0.4 mg PI in 50 mL of PBS and 0.5 mg FDA in 50 mL of acetone. The solution was kept at 4°C until needed.

Nanoparticles Sterile PCOOH-AuNPs obtained from Mintek (Randburg, South Africa) were provided as 50 mL aliquots at a concentration of 4.1 nM in suspension in milli-Q water. The sterility of the samples was confirmed by the microbiology section at the NIOH, after which they were kept at 4°C until needed. Nanoparticles were suspended in culture medium to reach desired concentrations (Section 2.8) directly prior to experimentation.

Phosphate-buffered saline Fluorescent Treponemal Antibody (FTA) hemagglutination buffer (phosphate-buffered saline [PBS]) was procured from Becton, Dickinson and Company (Sparks, MD, USA) as a dry powder. This was prepared for use as a 0.1 M PBS solution by dissolving 9.23 g in 1 L dH2O, then autoclaving for sterility. The solution was stored at room temperature until use.

Penicillin-streptomycin Penicillin-streptomycin solution, procured from Merck (Darmstadt, Germany), was stored in 5 mL aliquots at -20°C until thawed and dissolved in medium prior to use, as described in Section 2.5.

CytoTox-ONE™ Homogenous Membrane Integrity Assay All reagents were procured as a pre-prepared kit from Promega (Madison, WI, USA), and stored at -20°C in the dark until use. The kit contained 2 vials of substrate mix, 24 mL assay buffer, 0.5 mL lysis solution and 11 mL stop solution.

Dulbecco's Modified Eagle Medium

Gibco™ (Life Technologies Limited, Paisley, UK) Dulbecco's Modified Eagle Medium (DMEM) cell culture medium was procured from ThermoFisher (Johannesburg, South Africa), sterile, in pre-prepared 500 mL bottles and stored at 4°C until use. Sterile penicillin-streptomycin solution, L-glutamine, and heat-inactivated foetal calf serum (FCS) were added when needed to concentrations of 1% and 10% in medium, respectively. This was done by removing 55 mL of medium, then adding 5 mL of penicillin-streptomycin solution and 50 mL of FCS to the medium for a final volume of 500 mL.

Sodium azide

Sodium azide was procured from Merck (Darmstadt, Germany) as a dry powder and stored at 20°C. To make a 300 mM solution, 9.75 mg of dry powder was dissolved in 500 µL dH2O. Aliquots of 500 µL were stored at -80°C.

Sodium dodecyl sulphate

Sodium dodecyl sulphate (SDS) was procured from Merck (Darmstadt, Germany) as a dry powder and stored at room temperature. To make a 6.25% w/v solution, 6.25 g of dry powder was dissolved in 100 mL dH2O. The solution was stored at 4°C.

Tissue-Tek® O.C.T. Compound

Tissue-Tek® was procured from Sakura Finetek, Torrance, CA, USA and used as is. It was stored at room temperature until needed.

TrypLE™ Express Enzyme

TrypLe™ Express Enzyme (phenol red free) was procured from ThermoFisher (Johannesburg, South Africa) as a 500 mL bottle of pre-prepared solution ready for use. It was kept at 4°C until needed.

Appendix III: Supplementary data

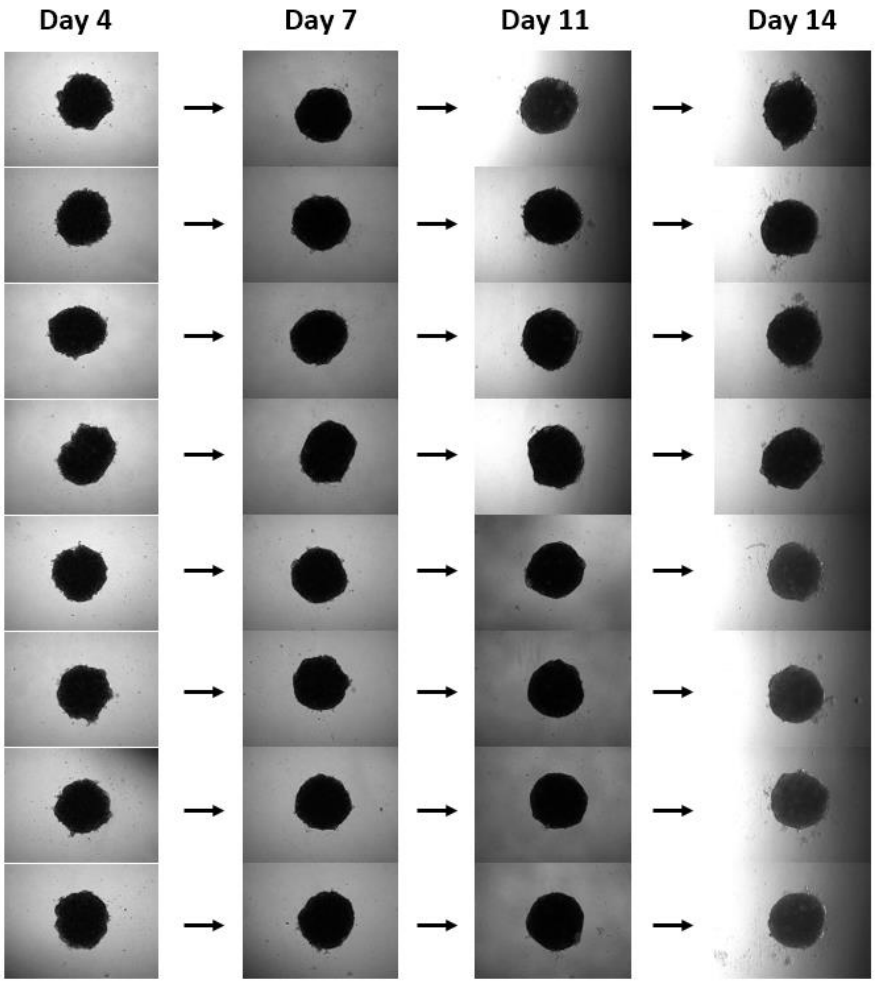

	Day 4	Day 7	Day 11	Day 14
Mean diameter (µm)	672.04	684.01	696.18	704.99
Mean circularity index	0.71	0.79	0.85	0.83